NASA Contractor Report 191048

Interactive Reliability Model for Whisker-Toughened Ceramics

Joseph L. Palko
Cleveland State University
Cleveland, Ohio

April 1993

Prepared for
Lewis Research Center
Under Grant NCC3–81

National Aeronautics and Space Administration

INTERACTIVE RELIABILITY MODEL FOR WHISKER-TOUGHENED CERAMICS

Joseph L. Palko
Cleveland State University
Cleveland, Ohio

ABSTRACT

Wider use of ceramic matrix composites (CMC) will require the development of advanced structural analysis technologies. This report focuses on the use of an interactive model to predict the time-independent reliability of a component subjected to multiaxial loads. The deterministic, three-parameter Willam-Warnke failure criterion serves as the theoretical basis for the reliability model. The strength parameters defining the model are assumed to be random variables, thereby transforming the deterministic failure criterion into a probabilistic criterion. The ability of the model to account for multiaxial stress states with the same unified theory is an improvement over existing models. The new model has been coupled with a public-domain finite element program through an integrated design program. This allows a design engineer to predict the probability of failure of a component. A simple structural problem is analyzed using the new model, and the results are compared to existing models.

CHAPTER I

INTRODUCTION

The ability of structural components, fabricated from both monolithic and composite ceramic material systems, to maintain their structural integrity while subjected to thermomechanical loads is beginning to capture the attention of many design engineers. Attractive properties such as low density, high strength, high stiffness, creep resistance, and corrosion resistance are allowing ceramic materials to supplant metal alloys in numerous applications. Current applications include heat exchangers, cutting tools, and wear parts. Larsen and Vyas (1988), Buljan, Pasto, and Kim (1989), and Clarke (1990) present commercial data regarding the expanding use of ceramic components for these rigorous applications. Unlike some metal alloys used in demanding service conditions (notably the superalloys), ceramic components are fabricated from nonstrategic materials. This has helped spur research efforts in both processing technology and structural analysis. This report focuses on issues related to the field of structural analysis, where design protocols are replacing the ad hoc trial-and-error method of developing and testing structural prototypes.

In the field of material science, efforts to improve the structural performance of ceramic materials include adding a second ceramic phase to the matrix. This second phase can take the form of whiskers, short (usually chopped) fibers, continuous fiber reinforcement, and woven fabrics. This report will focus on ceramic composites that incorporate whisker reinforcement (and under certain conditions, particulate reinforcement). The addition of whiskers improves the failure behavior of the material system by arresting crack growth in the matrix by pinning, bridging, and deflecting cracks. The improvement of fracture toughness, usually in certain material directions, is dependent on processing. As a result, this material can exhibit anisotropic behavior. However, if the whiskers are homogeneously distributed and randomly oriented, the isotropic nature of the matrix material is preserved. The work presented here will deal exclusively with the isotropic whisker-toughened material system. Analytical efforts that allow for material anisotropy are mentioned in chapter V.

Even though the second phase enhances the failure behavior of the material, whisker-toughened ceramics still fail in a brittle fashion. In addition, there is a great deal of intrinsic variability in the strength of this material. Failure of structural components fabricated from whisker-toughened ceramics is governed by random flaw populations inherent to the material's microstructure. Usually these material imperfections are generated during processing. It is assumed that the location and orientation of the flaws are randomly distributed

throughout a component. The resulting scatter in failure strength of these materials requires a departure from traditional design philosophies. The random nature of the microstructural flaws forces the design engineer to rethink the design philosophy that treats material strength as a single-valued design parameter. For monolithic ceramics, the factor of safety approach (a deterministic design procedure commonly used for metal alloys) has been abandoned in favor of a reliability-based approach. Work by Gyekenyesi (1986), Cooper, Margetson, and Humble (1986), and Lamon (1990) are representative of the reliability design philosophy used in analyzing structural components fabricated from monolithic ceramics.

Adopting a similar probabilistic philosophy for the structural analysis of a component fabricated from whisker-toughened material allows the design engineer to account for brittle behavior, variability in strength, and decreasing bulk strength with increasing component volume (the so-called size effect). Using probabilistic methods, the component is discretized using finite element techniques, and each discrete element is treated as a link in a chain. Philosophically, this means that when one element fails, the component fails. Thus the component is only as strong as the weakest link in the chain. From the standpoint of reliability theory, the component is treated as a series system, where failure of the system occurs when one of the subsystems fails. Alternatively, in a parallel system, failure of a single subsystem does not cause the system to fail since the remaining elements of the system may sustain load through redistribution. Models that use the analogy of a parallel system lead to what has been referred to in the literature as bundle theories. The basic principles underlying bundle theories were originally discussed by Daniels (1945) and Coleman (1958). Bundle theories have been applied exclusively to long-fiber ceramic composites. Thus, further discussion of these theories will not be pursued here. See the work of Harlow and Phoenix (1981), and Phoenix (1974, 1979) for an in-depth treatment of the bundle theory.

In general, two categories of weakest link theories have emerged. One group is based on the principles of fracture mechanics. The other group adopts a phenomenological viewpoint. The fracture mechanics approach assumes that the stress state in the near vicinity of the critical crack and the orientation of the crack are the controlling design variables. Material strength and crack orientation are treated as random variables. All other design variables (e.g., load, geometry, stiffness, etc.) are treated in a deterministic fashion. In contrast, phenomenological reliability models take a more global approach. Only material strength is treated as a random variable since attention is not focused on a critical flaw. Phenomenological models can be either interactive or noninteractive. Interactive models allow functional forms that include terms that are products of different material strengths. Noninteractive theories allow material strength parameters to appear only as separate and distinct terms. Throughout this report, the fracture mechanics and the phenomenological criterion will be discussed for the purpose of comparison, but the attention will be focused mainly on interactive models. In chapter II, a literature survey is presented that outlines different methods of modeling reliability.

With the exception of the work by Adams and Sines (1978), Alpa (1984), and Powers (1989), reliability theories for ceramic components have neglected compressive stress states and the effect of hydrostatic stress in particular. Models such as the principle of independent action (PIA), which was originally proposed by Barnett et al. (1967) and Freudenthal (1968), and the familiar Batdorf theory (Batdorf and Crose, 1974) do not allow compressive states of stress to influence component reliability. Since the compressive strength of ceramic materials is often an order of magnitude larger than the tensile strength, compressive stress states were assumed not to contribute to failure, or treated in an ad hoc fashion in a manner similar to Gyekenyesi (1986). Although data in the open literature are limited, experimental evidence by Adams (1975), Ikeda and Igaki (1984) and Ikeda, Igaki, and Kuroda (1986) clearly indicates that compressive stress states have a decided effect on ceramic materials. The phenomenological criterion that is discussed later allows for multiaxial states of stress, and specifically treats compressive stress in a rational manner as outlined in chapter IV. The criterion (and the reliability model that is derived from this criterion) is unified in the sense that ad hoc rules are not used to model different regions in the stress state. The analytical details of the parent deterministic failure model are

given in chapter III. Failure surfaces projected into various stress spaces are presented to illustrate different mechanistic aspects of the theory. Finally, the tests necessary to determine the parameters are outlined.

Casting the deterministic failure theory into a reliability model using Monte Carlo methods is presented in chapter IV. Numerical aspects of the Monte Carlo simulation are discussed. Features of the interactive reliability model are compared with existing models. The reliability model is incorporated into a test-bed software program given the acronym TCARES (Toughened Ceramics Analysis and Reliability Evaluation of Structures), which was originally discussed by Duffy et al. (1989). Coupling the reliability algorithm with a general-purpose finite element program (i.e., MSC/NASTRAN) enables one to predict the time-independent reliability of a structural component. A structural component is analyzed that illustrates the interactive model highlighted in this report. These results are compared with an analysis made using previous models that did not allow compressive stress states to affect component reliability. It is shown that these previous models yield unconservative results in certain situations.

Chapter V summarizes this effort and indicates future research. Future direction includes improving numerical efficiency through the use of fast probability integration techniques proposed by Wu (1984). Applying this type of analysis to anisotropic whisker-toughened ceramics is outlined.

CHAPTER II

SURVEY OF RELIABILITY THEORIES

Traditional failure analyses of structural components have used deterministic approaches where failure is assumed to occur when some allowable stress level, or equivalent quantity, is exceeded. This assumes that deformation is not controlling component design. Since structural ceramics maintain high stiffness, even at elevated temperatures, deformation has not played a significant role in component design. Certain design methods have attempted to incorporate the relevant physics of failure using fracture mechanics. Here the critical design parameter is the stress intensity factor, which takes into account load and component geometry. In this approach the stress intensity factor is compared to a fracture toughness value that is a characteristic property of the material. However, for most structural ceramics the combination of ultimate strength and fracture toughness (quantified by K_{1C}) yields flaw sizes so small that current nondestructive evaluation (NDE) methods are unable to detect the critical defect. On the other hand, phenomenological failure theories make use of macroscopic strength parameters that do not focus on a critical microstructural defect. Multiaxial failure theories can be systematically formulated using this approach if the material is homogeneous, with strength properties that can be deduced from well chosen phenomenological experiments. Failure theories such as the maximum normal stress, the maximum normal strain, the maximum shear stress, and the maximum distortional energy criteria are examples of phenomenological models that are successful in predicting the onset of brittle failure or yielding. However, for reasons mentioned in the introduction, these deterministic techniques are not relevant when analyzing structural components fabricated from ceramic-based material systems.

Weibull (1939, 1951) proposed the first probabilistic model that accounted for scatter in failure strength and the size effect encountered in brittle materials. His approach is based on the weakest link theory (WLT) attributed to Midgley and Pierce (1926). This earlier research (sponsored by the textile industry) focused on modeling yarn strength. Unlike Midgley and Pierce, who assumed a Gaussian distribution for yarn strength, Weibull proposed a unique probability density function for failure strength that now bears his name. Weibull's two-parameter probability density function has the following form:

$$f(x) = \left[\frac{\alpha}{\beta}\right]\left[\frac{x}{\beta}\right]^{(\alpha-1)} \exp\left[-\left[\frac{x}{\beta}\right]^{\alpha}\right] \tag{2.1}$$

for a continuous random variable x, when $x > 0$, and

$$f(x) = 0 \tag{2.2}$$

for $x \leq 0$. The cumulative distribution function is given by the expression

$$F(x) = 1 - \exp\left[-\left[\frac{x}{\beta}\right]^{\alpha}\right] \tag{2.3}$$

for $x > 0$, and

$$F(x) = 0 \tag{2.4}$$

for $x \leq 0$. Here α (> 0) is the Weibull modulus (or the shape parameter), and β (> 0) is the scale parameter. Reliability theories with theoretical frameworks based on Weibull's original concepts are presented in this chapter. Theories based on phenomenological principles and fracture mechanics theories are discussed. Initially, Weibull's (1939) normal stress averaging technique is presented. This is followed by a discussion of the PIA model, and recent extensions of the PIA model to composite materials. Next, a reliability model developed by Batdorf and Crose (1974), founded on principles of fracture mechanics, is presented. Finally, a model that accounts for compressive states of stress (Powers, 1989) is discussed.

Weibull's Normal Stress Averaging Method

Weibull adopted the weakest link theory where a brittle material is considered a chain with links connected in series. The overall strength of a brittle component is then governed by the strength of its weakest link. Focusing on a single link, the failure probability of an individual link can be expressed as

$$P_f = \psi \Delta V \tag{2.5}$$

where ΔV is the volume of the link, and ψ is a failure function per unit volume of material. By defining r as the reliability of a single link, then

$$r = 1 - \psi \Delta V \tag{2.6}$$

The failure of an individual link is assumed to be an independent statistical event, implying that the events leading to failure of an individual link are not influenced by other links in the chain. As a result, the reliability of the component, denoted as R, becomes

$$R = \lim_{N \to \infty} \left[\prod_{\lambda=1}^{N} r_\lambda \right] = \lim_{N \to \infty} \left[\prod_{\lambda=1}^{N} \left[1 - \psi(\sigma_{ij}, x_i) \Delta V \right]_\lambda \right] \tag{2.7}$$

where N is the number of links in the component, $\psi(\sigma_{ij}, x_i)$ is the failure function per unit volume at position x_i within the component, and σ_{ij} is the Cauchy stress tensor at x_i. Unless noted otherwise, lowercase Roman letter subscripts in italics denote tensor indices with an implied range from 1 to 3, and Greek letter subscripts are associated with products or summations with ranges that are explicit in each expression. By adopting the argument originally proposed by Weibull, the reliability of the component takes the integral form

$$R = \exp\left[- \int_V \psi(\sigma_{ij}, x_i) dV \right] \tag{2.8}$$

where V is the volume of the component. Similarly, the probability of failure for the component takes the form

$$P_f = 1 - R = 1 - \exp\left[- \int_V \psi(\sigma_{ij}, x_i) dV \right] \tag{2.9}$$

The state of stress in every link of the chain must be characterized to conduct a reliability analysis using equation (2.8). This approach lends itself to analytical techniques that use finite element methods. If a component is modeled as a chain with individual links connected in series, then each link would correspond to an element within a mesh. The reliability models that are discussed in this section, and in later sections, adopt

this theoretical framework (eqs. (2.5) to (2.9)) in computing component reliability, and all are amenable to finite element methods. The differences between various reliability models occur in the formulation of the failure function ψ.

Weibull assumed that the failure strength of a specimen subjected to a uniaxial state of stress is a random variable. Application of equation (2.9) for a uniaxial tensile stress field in a homogeneous isotropic material yields

$$P_f = 1 - \exp\left[-\left(\frac{\sigma}{\beta}\right)^{\alpha} V\right] \tag{2.10}$$

where σ is the applied tensile stress, and V is the volume of the specimen. For this case Weibull took the failure function (ψ) as

$$\psi = \left(\frac{\sigma}{\beta}\right)^{\alpha} = k\sigma^{\alpha} \tag{2.11}$$

Here k is referred to in the literature as Weibull's coefficient for a uniaxial state of stress. Weibull extended this uniaxial model to multiaxial states of stress by defining an average tensile stress. He defined this average tensile stress by considering the stress traction on an arbitrary plane (see fig. 2.1). Specifically the shear component of the stress traction $\tilde{\tau}$ is ignored, and it is assumed that only the normal component $\tilde{\sigma}$ causes failure. To gain a clear understanding of this method, consider a sphere centered at the origin of the coordinate axis (x_1, x_2, x_3) associated with the principal directions σ_1, σ_2, and σ_3. The normal component of stress traction acting on an arbitrary plane is given by the expression

$$\tilde{\sigma} = \sin^2\phi\left(\sigma_1 \cos^2\theta + \sigma_2 \sin^2\theta\right) + \sigma_3 \cos^2\phi \tag{2.12}$$

Here ϕ and θ are the polar and azimuthal angles of the unit vector normal to the arbitrary plane in stress space. These angles and their relationship to the coordinate axes (x_1, x_2, x_3) are shown in figure 2.2. Since the normal stress component varies with each planar orientation defined by ϕ and θ, Weibull defined the following weighted average

$$(\bar{\sigma})^{\alpha} = \frac{8\int_0^{\pi/2}\int_0^{+\theta}\tilde{\sigma}^{\alpha}\sin\phi\, d\theta\, d\phi}{\int_A dA} \tag{2.13}$$

Here A is the area of the unit sphere, and the limits of θ coincide with those orientations where $\tilde{\sigma}$ changes from a tensile stress to a compressive stress. For the limiting case where $\tilde{\sigma}$ is tensile over the entire sphere, θ takes the value of $\pi/2$. Both limits are zero if $\tilde{\sigma}$ is compressive over the entire unit sphere, and this results in $(\bar{\sigma})^{\alpha} = 0$. The general convention analyzes this integral over one octant of the unit sphere, which accounts for the limits of integration for ϕ (i.e., 0 and $\pi/2$), and the factor 8 in the numerator.

The quantity $(\bar{\sigma})^{\alpha}$ given by equation (2.13) is equated to σ^{α} in equation (2.11) such that

$$\psi = k(\bar{\sigma})^{\alpha} \tag{2.14}$$

where k is Weibull's coefficient for a multiaxial stress state. This coefficient is the multiaxial extension of the parameter k defined in equation (2.11), and must be defined in a consistent fashion such that equation (2.14) yields equation (2.11) for a uniaxial state of stress. Equating Weibull's multiaxial formulation of ψ defined in equation (2.14) to the uniaxial case defined in equation (2.11) results in the following relationship (see Gyekenyesi (1986) for details):

$$k = k(2\alpha + 1) = \frac{(2\alpha + 1)}{\beta^{\alpha}} \tag{2.15}$$

Thus for the multiaxial state of stress,

$$P_f = 1 - \exp\left[-\int_V k(\bar{\sigma})^{\alpha} dV\right] \tag{2.16}$$

from which the uniaxial form expressed in equation (2.10) can be obtained. Although the extension to multiaxial states of stress described here is intuitively plausible, it is somewhat arbitrary because it disregards the shear component of the stress traction. In addition, since the method lacks a closed-form solution, use of this model requires computationally intensive numerical methods.

Principle of Independent Action Method

Barnett et al. (1967) and Freudenthal (1968) proposed an alternative to Weibull's normal stress averaging approach for multiaxial states of stress. Here only principal stresses are considered, and the basic assumption is that each acts independently in reducing the survival probability of an element (hence the name principal of independent action). The failure function for this theory takes the form

$$\psi = \left[\frac{\sigma_1}{\beta}\right]^{\alpha} + \left[\frac{\sigma_2}{\beta}\right]^{\alpha} + \left[\frac{\sigma_3}{\beta}\right]^{\alpha} \tag{2.17}$$

where $\sigma_1 \geq \sigma_2 \geq \sigma_3 \geq 0$. Since the principal stresses appear in separate terms (i.e., they do not interact) in the formulation of ψ, this model is classified as a noninteractive reliability model. Qualitatively, the PIA theory is equivalent in a probabilistic sense to the maximum stress failure theory.

Extensions of the PIA Method

Duffy and Arnold (1990) formulated an extension of the PIA model for transversely isotropic materials. A unit vector was used to identify the local material orientation, and, subsequently, to define stress invariants. The unit vector d_i was introduced to define the direction normal to the plane of isotropy. Here the failure function ψ depends on the stress state and local material orientation such that

$$\psi = \psi\left(\sigma_{ij},\, d_i\right) \tag{2.18}$$

Since ψ is a scalar valued function, it must remain form invariant. To ensure this, an integrity basis was developed for ψ that contained certain combinations of invariants of the Cauchy stress tensor and an orientation tensor defined as $d_i d_j$. The invariants formed an integrity basis and were used to construct other invariants that correspond to specific components of the state of stress in an element. This approach yields the following functional dependence

$$\psi = \psi\left(\hat{I}_1, \hat{I}_2, \hat{I}_3, \hat{I}_4\right) \tag{2.19}$$

Here $\hat{I}_1$ corresponds to the magnitude of the stress vector $\sigma_{ij}d_j$ projected onto the material orientation vector d_i. The invariant $\hat{I}_2$ represents the magnitude of the shear component of the stress traction. The invariants $\hat{I}_3$ and $\hat{I}_4$ represent the magnitudes of the maximum and minimum principal stresses in the plane of isotropy. Thus each invariant corresponds to a strength in a well-defined material direction, and because of this the invariants can be treated as random variables with underlying Weibull distributions. Analogous to the principle of independent action, it is assumed that the different invariants are statistically independent such that the failure function takes the form

$$\psi = \left[\frac{\langle \hat{I}_1 \rangle}{\beta_1}\right]^{\alpha_1} + \left[\frac{|\hat{I}_2|}{\beta_2}\right]^{\alpha_2} + \left[\frac{\langle \hat{I}_3 \rangle}{\beta_3}\right]^{\alpha_3} + \left[\frac{\langle \hat{I}_4 \rangle}{\beta_3}\right]^{\alpha_3} \tag{2.20}$$

where the individual α's and β's are the Weibull parameters associated with a strength variable in a particular material direction. It should be noted that compressive stresses associated with $\langle \hat{I}_1 \rangle$, $\langle \hat{I}_3 \rangle$, and $\langle \hat{I}_4 \rangle$ are assumed not to contribute to a reduction in reliability such that

$$\langle \hat{I}_1 \rangle = \begin{cases} \hat{I}_1 & \hat{I}_1 > 0 \\ 0 & \hat{I}_1 \le 0 \end{cases} \tag{2.21}$$

$$\langle \hat{I}_3 \rangle = \begin{cases} \hat{I}_3 & \hat{I}_3 > 0 \\ 0 & \hat{I}_3 \le 0 \end{cases} \tag{2.22}$$

and

$$\langle \hat{I}_4 \rangle = \begin{cases} \hat{I}_4 & \hat{I}_4 > 0 \\ 0 & \hat{I}_4 \le 0 \end{cases} \tag{2.23}$$

Duffy and Manderscheid (1990) formulated an extension of the PIA model for orthotropic materials. Here two mutually orthogonal unit vectors (a_i and b_i) were used to define local material directions. An integrity basis was developed from the functional dependence

$$\psi = \psi\left(\sigma_{ij}, a_i b_j\right) \tag{2.24}$$

where $a_i b_j$ serves as a direction tensor. Like the transversely isotropic case, the failure function depends on certain invariants that correspond to components of the local stress tensor; that is,

$$\psi = \psi\left(\tilde{I}_1, \tilde{I}_2, \tilde{I}_3, \tilde{I}_4, \tilde{I}_5\right) \tag{2.25}$$

Here the invariants $\tilde{I}_1$ and $\tilde{I}_3$ represent the magnitude of the normal stress components in the directions of a_i and b_i, respectively. The invariants $\tilde{I}_2$ and $\tilde{I}_4$ represent the shear stresses across the directions a_i and b_i respectively. The invariant $\tilde{I}_5$ represents the normal stress in the direction defined by the cross product of the vectors a_i and b_i. Once again, it is assumed that the invariants are statistically independent such that

$$\psi = \left[\frac{\langle \tilde{I}_1 \rangle}{\beta_1}\right]^{\alpha_1} + \left[\frac{|\tilde{I}_2|}{\beta_2}\right]^{\alpha_2} + \left[\frac{\langle \tilde{I}_3 \rangle}{\beta_3}\right]^{\alpha_3} + \left[\frac{|\tilde{I}_4|}{\beta_4}\right]^{\alpha_4} + \left[\frac{\langle \tilde{I}_5 \rangle}{\beta_5}\right]^{\alpha_5} \tag{2.26}$$

where the individual α's and β's are again associated with strength variables in particular material directions. The invariants $\tilde{I}_1$, $\tilde{I}_3$, and $\tilde{I}_5$ are normal stresses, and do not contribute to a reduction in reliability if they are compressive; that is,

$$\langle \tilde{I}_1 \rangle = \begin{cases} \tilde{I}_1 & \tilde{I}_1 > 0 \\ 0 & \tilde{I}_1 \le 0 \end{cases} \tag{2.27}$$

$$\langle \tilde{I}_3 \rangle = \begin{cases} \tilde{I}_3 & \tilde{I}_3 > 0 \\ 0 & \tilde{I}_3 \le 0 \end{cases} \tag{2.28}$$

and

$$\langle \tilde{I}_5 \rangle = \begin{cases} \tilde{I}_5 & \tilde{I}_5 > 0 \\ 0 & \tilde{I}_5 \le 0 \end{cases} \tag{2.29}$$

The reliability models for both the transversely isotropic and orthotropic materials allow the material orientation to vary along a family of curves within the component. Thus the material is locally anisotropic. The models were constructed using invariant formulations which indicate the maximum number and forms of the stress invariants necessary to define the failure function ψ. In both cases, a subset of the integrity basis for ψ

was constructed, resulting in reliability models that are similar in nature to the PIA reliability model for monolithic ceramics.

Batdorf's Theory–Surface Flaw Analysis

Reliability theories based on fracture mechanics assume that failure of a component emanates from a single flaw with a critical size and orientation. This flaw belongs to a population that in general contains surface flaws and volume flaws. Either type of flaw is assumed to be uniformly distributed and randomly oriented. Surface flaws are imperfections that are the result of machining, grinding, or other surface finishing operations. Volume flaws are the direct result of processing. Both types of flaw populations exhibit different failure behavior characterized by distinct strength distribution parameters. For surface flaws, the presence of a traction-free surface reduces a three-dimensional state of stress to a state of plane stress. Because of this simplifying condition, the details of a surface flaw analysis are presented. In general, the surface flaw analysis can be viewed as a special case of volume flaw analysis.

Batdorf and Heinisch (1978) proposed a surface flaw model which is an extension of an earlier volume flaw analysis proposed by Batdorf and Crose (1974). This two-dimensional theory is based on weakest link principles, and accommodates mode I, mode II, or mixed mode fracture criteria. For the following discussion, the coplanar strain energy release rate, a mixed mode criterion, is used. This criterion allows for mode I and mode II behavior, and takes the form

$$\left[\frac{K_I}{K_{IC}}\right]^2 + \left[\frac{K_{II}}{K_{IC}}\right]^2 = 1 \tag{2.30}$$

where K_I and K_{II} are the mode I and mode II stress intensity factors, respectively. These stress intensity factors are functions of the applied far-field stress state and the crack geometry. For a Griffith crack (a sharp through-crack of length 2a), the stress intensity factors for a two-dimensional infinite plate are

$$K_I = \sigma\sqrt{\pi a} \tag{2.31}$$

and

$$K_{II} = \tau\sqrt{\pi a} \tag{2.32}$$

Here σ is the far-field normal stress, and τ is the far-field shear stress. Substituting equations (2.31) and (2.32) into equation (2.30) yields the following expression:

$$\left[\frac{K_{IC}^2}{\pi a}\right]^{1/2} = \sqrt{\sigma^2 + \tau^2} \tag{2.33}$$

At this point, index notation is briefly suspended in order to use notation that has been widely accepted in discussing Batdorf's theory. By defining

$$\sigma_{cr} = \left[\frac{K_{1C}^2}{\pi a}\right]^{1/2} \tag{2.34}$$

as a critical stress, then equation (2.33) (together with eq. (2.34)) defines a failure envelope which is dependent on the material's fracture toughness and crack size. This failure envelope is shown in figure 2.3. Since the size (denoted as "a" in the denominator of eq. (2.34)) and orientation of the critical crack will vary, σ_{cr} represents a random variable. Thus there is a family of failure envelopes corresponding to each value of the random variable σ_{cr}. Batdorf used this concept to transform a deterministic fracture criterion into a reliability model.

The Batdorf theory stipulates that the probability of failure of a single link is the product of two probabilities; that is,

$$p_f = p_1 p_2 \tag{2.35}$$

Here p_1 is the probability that a crack exists such that the applied stress is in the range of σ_{cr} to $(\sigma_{cr} + d\sigma_{cr})$. This probability is defined by the expression

$$p_1 = \Delta A \left[\frac{dN(\sigma_{cr})}{d\sigma_{cr}}\right] d\sigma_{cr} \tag{2.36}$$

where ΔA is the differential area of the link, and $N(\sigma_{cr})$ is a crack density function (i.e., N has units of cracks per unit area). The crack density function is defined as

$$N(\sigma_{cr}) = k_B \sigma_{cr}^{\alpha} \tag{2.37}$$

and quantifies the number of cracks per unit area with an applied far-field stress that is greater than or equal to σ_{cr}. Here k_B is the Batdorf constant (which is functionally dependent on the Weibull scale parameter) and α is the Weibull modulus of the material. Both parameters can be determined experimentally by using the parameter estimation techniques outlined in Pai and Gyekenyesi (1988).

The quantity p_2 is the probability that a crack is oriented such that the critical stress is exceeded by an applied far-field stress. To illustrate this point, consider a state of plane stress using Mohr's circle where $0 < \sigma_2 < \sigma_1$ (see fig. 2.3). Define the angle ω as the initial orientation of the crack where the critical stress is exceeded. Note that the crack orientation varies between 0 and 2π radians, and there may be more than one orientation where the critical stress is exceeded. Next, overlay the fracture envelope expressed in equation (2.33) on the same set of axes. The angle between the σ axis and the line OA defines 2ω. Here point O is the center of Mohr's circle defined by the in-plane principal stresses σ_1 and σ_2. Point A is the intersection of the failure envelope given by equation (2.33) and Mohr's circle and defines the initial orientation of a crack where the critical stress is exceeded. Any point on Mohr's circle outside the failure envelope represents a possible failure stress state. Thus the probability that a crack is oriented such that the critical stress is exceeded by the applied far-field stress is

$$p_2 = \frac{\omega}{\pi/2} \tag{2.38}$$

where $0 \leq p_2 \leq 1$.

The geometry in figure 2.3 is used to established the form of equation (2.38). The applied far-field stress is equal to σ_{cr} at point A; thus

$$\omega = \cos^{-1}\left[\frac{\sigma_{cr}^2 - \sigma_2^2}{\sigma_1^2 - \sigma_2^2}\right]^{1/2} \tag{2.39}$$

Hence,

$$p_2 = \frac{2}{\pi}\cos^{-1}\left[\frac{\sigma_{cr}^2 - \sigma_2^2}{\sigma_1^2 - \sigma_2^2}\right]^{1/2} \tag{2.40}$$

when $\sigma_2 \leq \sigma_{cr} \leq \sigma_1$, and

$$p_2 = 1 \tag{2.41}$$

when $\sigma_{cr} \leq \sigma_2$. For the case where $\sigma_2 < \sigma_1 < \sigma_{cr}$,

$$p_2 = 0 \tag{2.42}$$

Following the argument outlined in equations (2.5) to (2.7), with the results of equations (2.36) and (2.40), then the reliability of a component is given as

$$R = \exp\left[-\int_A \int_0^{\sigma_1} \left[\frac{dN(\sigma_{cr})}{d\sigma_{cr}}\right] \frac{2\omega}{\pi}\, d\sigma_{cr} dA\right] \tag{2.43}$$

Similarly, the probability of failure of a component becomes

$$P_f = 1 - \exp\left[-\int_A \int_0^{\sigma_1} \left[\frac{dN(\sigma_{cr})}{d\sigma_{cr}}\right] \frac{2\omega}{\pi}\, d\sigma_{cr} dA\right] \tag{2.44}$$

Note that the limit of integration defined by A is the area of the component, and the limits of integration for σ_{cr} assume that σ_1 is the largest principal stress. In the context of the preceding discussion concerning reliability models, the failure function for Batdorf's model is defined by the integral

$$\psi = \int_0^{\sigma_1} \left[\frac{dN(\sigma_{cr})}{d\sigma_{cr}} \right] \frac{2\omega}{\pi} \, d\sigma_{cr} \tag{2.45}$$

The above analysis assumes that compressive stresses do not contribute to failure. For discussion on Batdorf's model for a volume analysis, see Batdorf and Crose (1974).

Power's Extension of Batdorf's Theory

The Powers model (Powers, 1989) represents a hybrid approach to reliability analysis in the sense that Batdorf's approach is adopted to predict reliability of a single link when both of its principal stresses are tensile, and the Mohr-Coulomb failure theory is used when both are compressive. When one principal stress is tensile and the other is compressive, a transition from the phenomenological criterion to the fracture criterion is necessary. The details concerning the transition are rather complex and will not be reviewed here. Thus the remainder of this section outlines the details of how Powers uses Mohr-Coulomb theory to predict reliability of monolithic ceramic components. Mohr-Coulomb theory defines failure when the shear stress on an unspecified failure plane reaches a critical value. Thus the shear stress at failure is a function of the coefficient of internal friction (μ), a compressive stress acting normal to the failure plane, and σ_{cr} (which was defined previously). The failure criterion takes the form

$$|\tau| + \mu\sigma = \sigma_{cr} \tag{2.46}$$

Powers assumes that the envelope for the Mohr-Coulomb failure criterion coincides with the envelope from Batdorf's fracture criterion at $\sigma = 0$, which results in $\tau = \sigma_{cr}$ at this point. This represents a major drawback and is discussed later. When viewed in Mohr's stress space, the Mohr-Coulomb failure envelope is linear; hence a slope and a point completely define the envelope. In her analysis, Powers specifies the slope as the material parameter μ. This quantity is defined as a single valued deterministic parameter. The associated point is the quantity σ_{cr} from Batdorf's analysis. This quantity is the only random variable in the analysis.

Powers defines an additional quantity σ_{max} in her analysis. When viewing a state of stress in Mohr's stress space, this represents the point where the failure envelope becomes tangent to Mohr's circle. In terms of the principal stresses and the parameter μ, σ_{max} takes the form

$$\sigma_{max} = \sqrt{1 + \mu^2} \, \frac{\sigma_1 - \sigma_2}{2} + \mu \, \frac{\sigma_1 + \sigma_2}{2} \tag{2.47}$$

Again, index notation is briefly suspended in order to use the notation as it appears in Powers' original work. This quantity is referred to as a "maximum" because it defines the limit of relevance from a reliability standpoint; that is, no reduction in reliability occurs if the failure envelope lies above this point.

The significance of σ_{max} is easily seen when deriving the failure function. Since plane stress conditions simplify the analysis, again only the details of a surface flaw analysis are presented. In a manner similar to Batdorf's approach, a critical stress and orientation of a failure plane must be defined in order to formulate the failure function. However, it must be emphasized that the Mohr-Coulomb theory makes no allowance for information concerning the physics of a crack (i.e., it is not a fracture criterion). Powers expresses the failure function as

$$\psi = \alpha k_B \sigma_{max}^{\alpha} \int_0^1 \bar{\omega} S_{cr}^{\alpha-1} dS_{cr} \tag{2.48}$$

where S_{cr} is a ratio of the critical stress (σ_{cr}) to the maximum stress (σ_{max}) for a given state of stress; i.e.,

$$S_{cr} = \frac{\sigma_{cr}}{\sigma_{max}} \tag{2.49}$$

The ratio S_{cr} facilitates the numerical integration of equation (2.48). By varying this ratio from 0 to 1, σ_{cr} is varied from 0 to σ_{max}. This guarantees that all relevant stress states are considered in the reliability prediction. Also note that $\bar{\omega}$ is similar in nature to the angle ω defined in equation (2.39) (the details will be discussed shortly), and the other terms in equation (2.48) have been defined in previous sections.

Several combinations of the failure envelope and Mohr's circle must be studied. Figure 2.4 shows that the failure envelope may not intersect Mohr's circle, the envelope may be tangent to the circle, or the envelope may intersect the circle at no more than two points. To determine the location of the intersection points and the portion of the circumference of Mohr's circle intersected, Powers formulates equation (2.46) in terms of the principal stresses, the ratio S_{cr}, and $\cos^2 \phi$. Here ϕ locates the intersection points on the circle. The equation now becomes quadratic in terms of $\cos^2 \phi$, and thus ϕ has two values, ϕ_1 and ϕ_2. The quantity $\bar{\omega}$, which appears in equation (2.48), is functionally dependent on the two angles ϕ_1 and ϕ_2 in the following manner:

$$\bar{\omega} = \frac{2(\phi_1 - \phi_2)}{\pi} \tag{2.50}$$

The angles ϕ_1 and ϕ_2 vary depending on the stress state. When there is no contact between the failure envelope and Mohr's circle (see fig. 2.4(a)), $\phi_1 = \phi_2 = 0$, and $\bar{\omega} = 0$. When the failure envelope and Mohr's circle are tangent at a point (fig. 2.4(b)), $\phi_1 = \phi_2 \neq 0$, and once again $\bar{\omega} = 0$. When the failure envelope intercepts Mohr's circle twice (fig. 2.4(c)), $\bar{\omega}$ represents the portion of Mohr's circle that lies outside of the failure envelope. With this interpretation of $\bar{\omega}$, and the definition of ψ given by equation (2.48), Powers' model yields the following expression

$$R = \exp\left[- \int_A \alpha k^B \sigma_{max}^{\alpha} \int_0^1 \bar{\omega} S_{cr}^{\alpha-1} dS_{cr} dA \right] \tag{2.51}$$

for component reliability when both principal stresses are negative.

The Mohr-Coulomb theory is a two-parameter failure theory that represents a straight line in the Mohr circle stress space. The slope and a point of intersection on the τ axis are used to define the linear envelope. Broad assumptions are made that μ is deterministic and σ_{cr} is a random variable. The effects of these assumptions are evident when comparing compression reliability predictions to tensile reliability predictions. Since μ is not treated as a random variable, the predicted scatter in strength (quantified by the Weibull modulus) is the same for simple compression and tensile tests using Powers' model. This result has never been supported by experimental data for a given material. In fact, intuition says that the scatter should be greatly reduced in compression. Thus the Weibull modulus for compression data should be substantially higher than the

Weibull modulus for tensile data. Accommodating this type of behavior is not a problem with the reliability model presented in chapter IV.

The following chapter presents the details of a three-parameter phenomenological failure model (the Mohr-Coulomb failure model is a two-parameter model). The method of transforming this deterministic phenomenological failure criterion into a reliability model is discussed in chapter IV. Basically, each of the three model parameters are treated as random variables with separate Weibull distributions. This leads to much greater flexibility in modeling reliability for multiaxial states of stress.

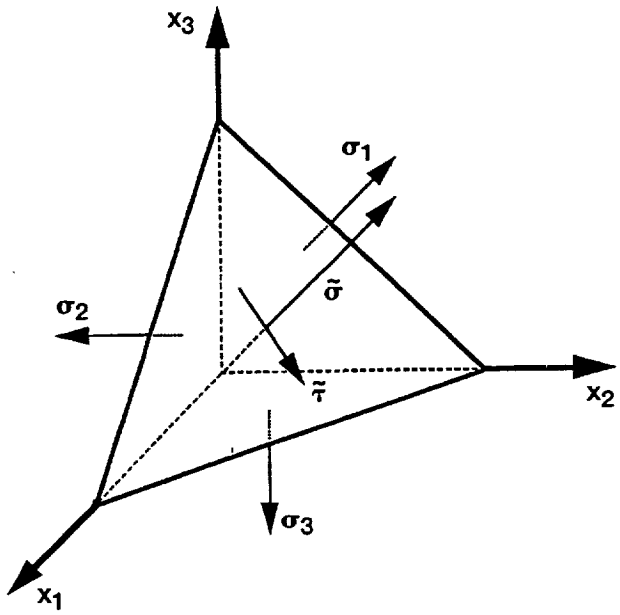

Figure 2.1.—Stress traction on an arbitrary plane.

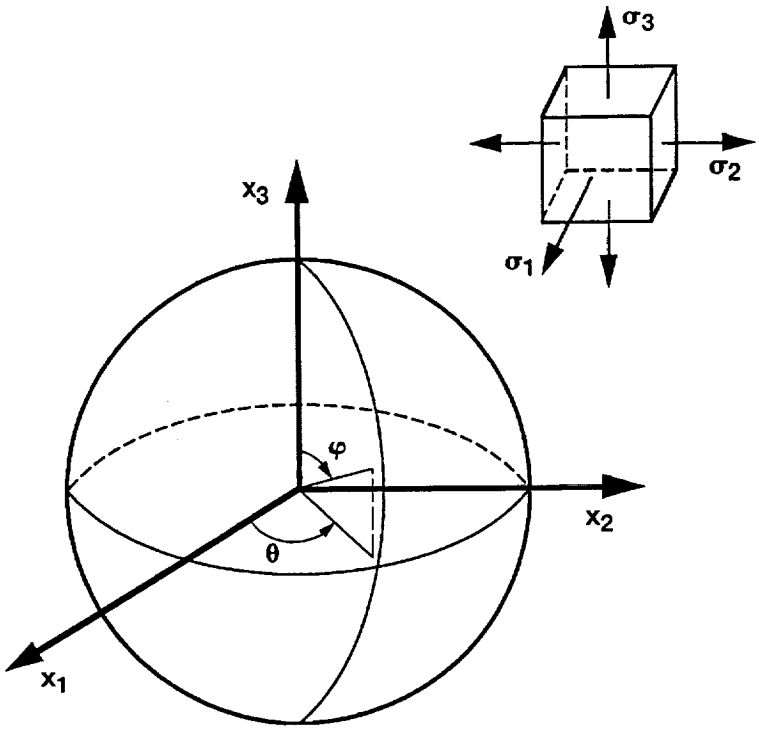

Figure 2.2.—Unit sphere in three-dimensional space.

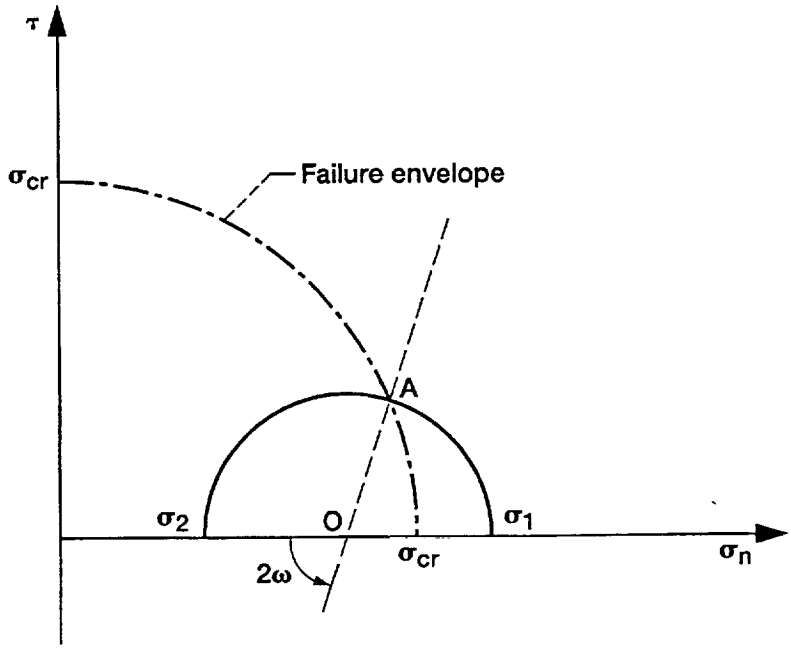

Figure 2.3.—Intersection of Mohr's circle and Batdorf's failure envelope.

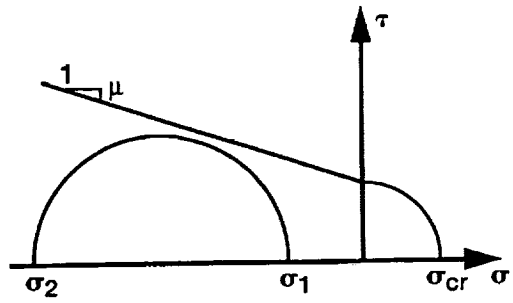

(a) No intersection between failure envelope and Mohr's circle.

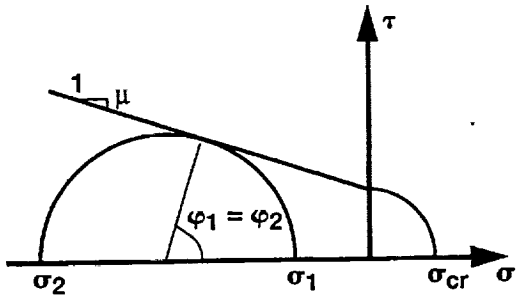

(b) Envelope tangent to circle at a point.

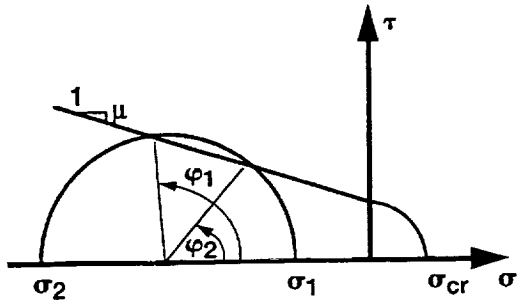

(c) Failure envelope cuts through Mohr's circle.

Figure 2.4.—Power's failure envelope and Mohr's circle.

CHAPTER III

WILLAM-WARNKE FAILURE CRITERION

A failure criterion defines a limit state. Within this limit state, a structural component will perform its design application in some acceptable fashion. A primary function of the design engineer is to define what is acceptable performance. Performance standards depend on the design variables used to define the limit state. Design variables, which may include strength parameters, cyclic load limits, and allowable deformation, can be assembled in an n-dimensional vector

$$\mathscr{Y}_\alpha = \left(Y_1, Y_2, \ldots, Y_n\right) \tag{3.1}$$

and the limit state function, which stipulates how the design variables interact, is expressed in general as

$$g\left(\mathscr{Y}_\alpha\right) = 0 \tag{3.2}$$

This function defines a surface in the n-dimensional design variable state. If a design point (i.e., an operational state where each design variable has a specified value) lies within the surface, then the design point represents a successful operational state. If the design point falls on the surface, the component fails. For deterministic analyses, points outside of the failure surface are inaccessible, since failure results once the surface is reached.

In this report, the design variable space, defined by the vector $\mathscr{Y}_\alpha$, is limited to strength parameters for ceramic material systems. Since strength parameters are associated with components of the Cauchy stress tensor, the general functional dependence of a limit state function is expressed as

$$g = g\left(\mathscr{Y}_\alpha, \sigma_{ij}\right) \tag{3.3}$$

where σ_{ij} represents the Cauchy stress tensor. A three-parameter strength criterion developed by Willam and Warnke (1975) will serve as the limit state function of primary interest here. The Willam-Warnke failure criterion (developed for isotropic materials) is a unified failure criterion in the sense that one limit state function defines failure for all regions of the stress space. As a comparison, Powers' model adopted Batdorf's theory for tensile regions of the stress space and Mohr-Coulomb theory for compressive regions of the stress space. The Willam-Warnke criterion uses stress invariants to define the functional dependence on the Cauchy stress σ_{ij}, specifically

$$g\left(\mathscr{Y}_\alpha, I_1, J_2, J_3\right) = 0 \tag{3.4}$$

This guarantees that the function is form invariant under all proper orthogonal transformations. Here I_1 is the first invariant of the Cauchy stress σ_{ij}, J_2 is the second invariant of the deviatoric stress S_{ij}, and J_3 is the third invariant of the deviatoric stress. These quantities are defined as

$$S_{ij} = \sigma_{ij} - \frac{1}{3}\delta_{ij}\sigma_{kk} \tag{3.5}$$

$$I_1 = \sigma_{kk} \tag{3.6}$$

$$J_2 = \frac{1}{2} S_{ij} S_{ji} \tag{3.7}$$

$$J_3 = \frac{1}{3} S_{ij} S_{jk} S_{ki} \tag{3.8}$$

where σ_{ij} is the identity tensor. Admitting I_1 to the function allows for a dependence on hydrostatic stress. The invariant J_3 allows different behavior in tension and compression since this invariant changes sign when the direction of a stress component is reversed.

Willam and Warnke defined the limit state function with the following expression

$$g\left(\mathscr{Y}_\alpha, I_1, J_2, J_3\right) = \lambda\left[\frac{\sqrt{J_2}}{Y_c}\right] + B\left[\frac{I_1}{Y_c}\right] - 1 \tag{3.9}$$

where

$$B = B\left(\mathscr{Y}_\alpha\right) \tag{3.10}$$

and

$$\lambda = \lambda\left(\mathscr{Y}_\alpha, J_3\right) \tag{3.11}$$

The functions B and λ will be defined momentarily. The strength parameters that comprise the design vector $\mathscr{Y}_\alpha$ include the uniaxial tensile strength of the material Y_t the equal biaxial compressive strength Y_{bc}, and the uniaxial compressive strength Y_c. This model is referred to as a three-parameter model, since three strength parameters, $\mathscr{Y}_\alpha = (Y_t, Y_c, Y_{bc})$, are used to define the limit state function. Failure occurs when $g = 0$ and the multiaxial criterion is completely defined in all regions of the six-dimensional stress space.

Since the limit state function is dependent on the six components of the Cauchy stress tensor, a design point and its relative position to the failure surface can be depicted in various stress spaces. Graphical representations can take place in a two- or three-dimensional stress space, using the components of the Cauchy stress tensor as coordinate axes. However, the function and the physical implications associated with the function can be viewed completely in the three-dimensional stress space where the principal stresses serve as orthogonal coordinate axes (see fig. 3.1(a)). This space is known as the Haigh-Westergard stress space. In this coordinate system, a given stress state, that is, a design point $P(\sigma_1, \sigma_2, \sigma_3)$, can be readily decomposed into hydrostatic and deviatoric components. This decomposition is shown in figure 3.1(b). Line d in figure 3.1(b) represents the hydrostatic axis where $\sigma_1 = \sigma_2 = \sigma_3$. Point P in this stress space represents an arbitrary state of stress. The vector NP represents the deviatoric component of the arbitrary stress state, and the vector ON represents the hydrostatic component.

The plane passing through the origin normal to the hydrostatic line is called the π-plane. For an isotropic material, a failure surface projected onto the π-plane must exhibit a sixfold symmetry. In the most general case where the isotropic material possesses equal strengths in tension and compression, the failure surface in the π-plane can be represented by two limiting cases (see fig. 3.2). The first case is represented by a circular failure surface, and the second is represented by a polygon inscribed within the circular failure surface. Any failure surface that does not fall within these two surfaces permits nonconvex regions to exist along the failure surface. However, proof of convexity also implies that level surfaces of a function are closed surfaces. An open region of the failure surface allows the existence of a load path along which failure will never occur. Thus for a convex surface, load paths cannot be traversed towards open regions of the failure surface, since open regions will not exist.

A failure surface projected onto the π-plane can be described conveniently with polar coordinates (r, θ). Here θ is defined as an angle measured clockwise from the σ_1-axis, and $r(\theta)$ is the distance from the hydrostatic axis to the failure surface (see fig. 3.2). Note that $r(\theta)$ is a function of θ for the inscribed polygon, and a constant for the circular failure surface. Physically, $r(\theta)$ represents the deviatoric component of a stress state, since this vector lies in the π-plane. In figure 3.2, the distance from the hydrostatic axis to the failure surface along a compressive principal axis r_c is equal to the distance along a tensile principal axis r_t for both limiting cases. However, ceramic material systems exhibit very different strengths in tension and compression. Failure models must account for this behavior, and this can be done simply by constructing the function $r(\theta)$ such that the intercepts along the tensile and compressive principal axes are different. The Willam-Warnke criterion accounts for this type of behavior by taking $r_c > r_t$ (see fig. 3.3).

As mentioned previously, isotropic materials must exhibit a sixfold symmetry in the π-plane. Willam and Warnke postulated that a single sector $(0 \le \theta \le \pi/3)$ of the failure surface in the π-plane could be represented as a segment of an ellipse. The major and minor axes of the ellipse were formulated as functions of the intercepts r_c and r_t (see fig. 3.4). Note that the minor axis of the ellipse is assumed to coincide with a tensile axis. However, the center of the ellipse does not necessarily coincide with the hydrostatic axis. The intercepts r_t and r_c depend on the strength parameters Y_t, Y_c, and Y_{bc}. Equations are given later that detail the interrelationships. In general the distance $r(\theta)$ is defined as

$$r(\theta) = \frac{2r_c\left(r_c^2 - r_t^2\right)\cos\theta + r_c\left(2r_t - r_c\right)\left[4\left(r_c^2 - r_t^2\right)\cos^2\theta + 5r_t^2 - 4r_t r_c\right]^{1/2}}{4\left(r_c^2 - r_t^2\right)\cos^2\theta + \left(r_c - 2r_t\right)^2} \tag{3.12}$$

where $0 \le \theta \le \pi/3$. A detailed derivation of this expression can be found in Chen (1982). Note that equation (3.12) yields $r(\theta) = r_t$ for the special case of $\theta = 0$. Similarly $r(\theta) = r_c$ for $\theta = \pi/3$.

With the definition of $r(\theta)$ given in equation (3.12), λ from equation (3.9) can be expressed as

$$\lambda = (2/5)^{1/2}\left[1/r(\theta)\right] \tag{3.13}$$

Here λ is implicitly dependent on J_3 through the angle θ. The dependence of θ on J_3 results from the similarities between the trigonometric identity

$$\cos^3\theta - \frac{3}{4}\cos\theta - \frac{1}{4}\cos(3\theta) = 0 \tag{3.14}$$

and the cubic equation used to find the deviatoric invariants

$$S^3 - J_2 S - J_3 = 0 \tag{3.15}$$

where the roots (S_1, S_2, S_3) are the eigenvalues of the deviatoric stress matrix. Substituting $S = \gamma \cos\theta$ into equation (3.15) yields

$$\cos^3\theta - \frac{J_2 \cos\theta}{\gamma^2} - \frac{J_3}{\gamma^3} = 0 \tag{3.16}$$

By comparing this expression with equation (3.14), it becomes apparent that

$$\gamma = \frac{2\sqrt{J_2}}{\sqrt{3}} \tag{3.17}$$

and

$$\cos(3\theta) = \frac{3\sqrt{3}\, J_3}{2\sqrt{(J_2)^3}} \tag{3.18}$$

The angle θ was first defined by Lode (1926), and the relationship between this angle and the deviatoric invariants was given by Nayak and Zienkiewicz (1972).

Details of the derivation for the Willam-Warnke criterion have been discussed in the context of the π-plane. Since the criterion is represented by a conic surface in the three-dimensional Haigh-Westergard stress space, and the function is sensitive to the hydrostatic component of the stress state, details obtained from the two-dimensional π-plane are not sufficient to completely describe the criterion. To gain a complete view of the criterion, a cutting plane is passed through the conic surface such that the entire length of the hydrostatic axis is contained in the cutting plane. This plane will intersect the surface along two lines. By definition, these lines are termed meridians.

Meridians define the profile of the conic failure surface in the Haigh-Westergard stress space. The relative position of each meridian is defined by the angle θ. For the tensile meridian $\theta = 0$, and for the compressive meridian $\theta = \pi/3$. In the π-plane, a compressive meridian is represented by point Q in figure 3.3, and a tensile meridian is represented by point T. For the Willam-Warnke criterion the meridians are linear, which is evident from the $I_1 - \sqrt{J_2}$ stress space in figure 3.5 and equation (3.9). Since the meridians are linear, two points on a meridian will define its position. For the tensile meridian the two points used to determine its position are defined by a uniaxial tensile load path, an equal biaxial compressive load path, and their intersection with the meridian. For both load paths equation (3.18) yields a value of $\theta = 0$. Considering a uniaxial tensile load case, failure results when σ_1 ($\sigma_1 = \sigma$) reaches Y_t (with $\sigma_2 = \sigma_3 = 0$). The load path for this case is defined by the ratio

$$\frac{I_1}{\sqrt{J_2}} = 1.73 \tag{3.19}$$

The value of I_1 (= σ) and $\sqrt{J_2}$ (= $\sigma/\sqrt{3}$) at failure will fix the position of one point on the meridian. In a similar fashion, the ratio

$$\frac{I_1}{\sqrt{J_2}} = 3.46 \tag{3.20}$$

defines the load path for equal biaxial compression where $\sigma_1 = \sigma_2$ (= σ) and $\sigma_3 = 0$. This load path fixes the position of a second point on the meridian. Here $I_1 = 2\sigma$ and $\sqrt{J_2} = \sigma\sqrt{(2/3)}$. Failure results when $\sigma_1 = \sigma_2 = Y_{bc}$. Both load paths are shown in figure 3.5. To clearly illustrate the load paths, the figure is not drawn to scale. The meridian is then defined by the line connecting these two points on the failure surface.

Similarly two points are used to determine the position of the compressive meridian. The points are defined by a uniaxial compressive load path and the intersection of the tensile meridian with the I_1-axis. The load path for the uniaxial compressive case is defined by the ratio

$$\frac{I_1}{\sqrt{J_2}} = 1.73 \tag{3.21}$$

where $I_1 = \sigma$ and $\sqrt{J_2} = (1/\sqrt{3})\,\sigma$. This path is shown in figure 3.5, and equation (3.18) yields a value of $\theta = \pi/3$. Failure results when $\sigma_1 = Y_c$ with $\sigma_2 = \sigma_3 = 0$. The second point on the compression meridian is the tip of the failure cone. Since the tensile meridian is completely defined by the parameters Y_t and Y_{bc}, the intersection of this line with the I_1 axis provides a second point for the location of the compressive meridian. This point is shown in figure 3.5 as point V. The distance ρ from point V to the origin represents the hydrostatic tensile stress at failure. Physically, this stress state is not easily produced in an experiment. However, this parameter is used to define B in equation (3.9). The parameter B is related to ρ by the simple expression

$$B = \frac{1}{3}\rho \tag{3.22}$$

As noted previously, the Willam-Warnke criterion is a three-parameter model. The parameters ρ, r_c, and r_t may be used to define the criterion in lieu of the strength parameters Y_c, Y_{bc}, and Y_t. The relationships are

$$\rho = \frac{y_{bc}\, y_t}{y_{bc} - y_t} \tag{3.23}$$

$$r_t = \left(\frac{6}{5}\right)^{1/2}\left[\frac{y_{bc}\, y_t}{2y_{bc} - y_t}\right] \tag{3.24}$$

and

$$r_c = \left(\frac{6}{5}\right)^{1/2}\left[\frac{y_{bc}\, y_t}{3y_{bc}y_t + y_{bc} - y_t}\right] \tag{3.25}$$

Here the expressions

$$y_{bc} = \frac{Y_{bc}}{Y_c} \tag{3.26}$$

and

$$y_t = \frac{Y_t}{Y_c} \tag{3.27}$$

are used to simplify equations (3.23) to (3.25). Once again, the derivations of these expressions were given by Chen (1982).

To gain further insight regarding physical implications of the criterion, consider the failure envelope projected onto the $\sigma_1 - \sigma_2$ stress plane, which is depicted in figure 3.6. Again this is a cutting plane that passes through the conic surface in the Haigh-Westergard stress space. Note that, in this figure, the function defines a smooth failure surface for any combination of the principal stresses. Also, the differences between the tensile strength and compressive strength of a material are readily apparent. The ratio of the intercepts along the tensile and the compressive axes is equal to the ratio of Y_t to Y_c. This stress space is encountered again in the next chapter, where reliability concepts are described.

Finally, the Willam-Warnke failure criterion degenerates to simpler models under special conditions. For the case of $r_c = r_t = r_o$, where r_o is the same for any angle θ, the surface degenerates to a circle in the π-plane and to a cone in the three-dimensional Haigh-Westergard stress space. This is the Drucker-Prager failure criterion, which is a two-parameter formulation. For the special case where $r_c = r_t = r_o$ and $\rho = \infty$, the model reduces to the single-parameter Von Mises criterion. For this case, the failure surface again becomes a circle in the π-plane, but a right circular cylinder in the three-dimensional Haigh-Westergard stress space. Since this criterion exhibits no dependence on hydrostatic stress, its meridians never intersect the I_1-axis in the $I_1 - \sqrt{J_2}$ stress space.

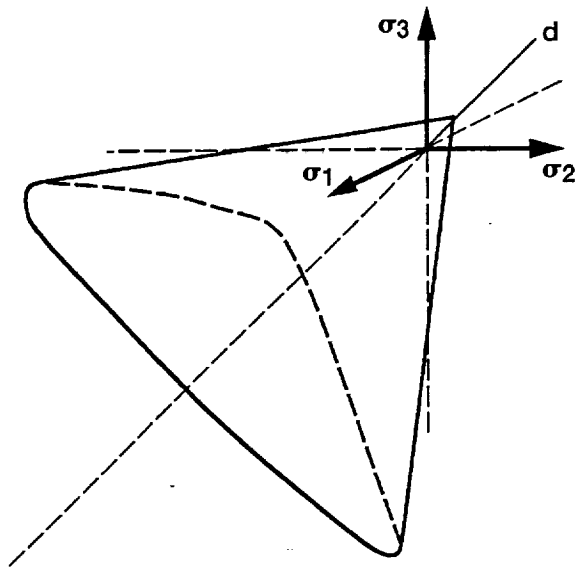

(a) Generalized failure surface in principal stress space.

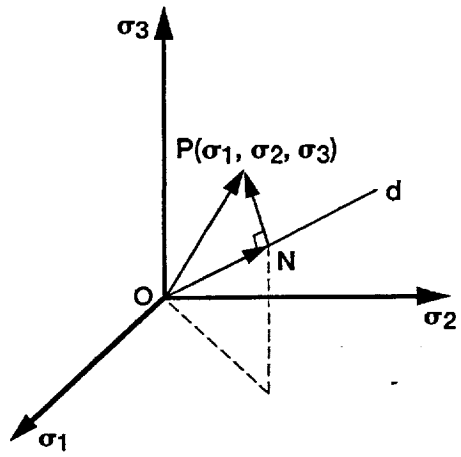

(b) Stress at a point in principal stress space.

Figure 3.1.—Principal stress space.

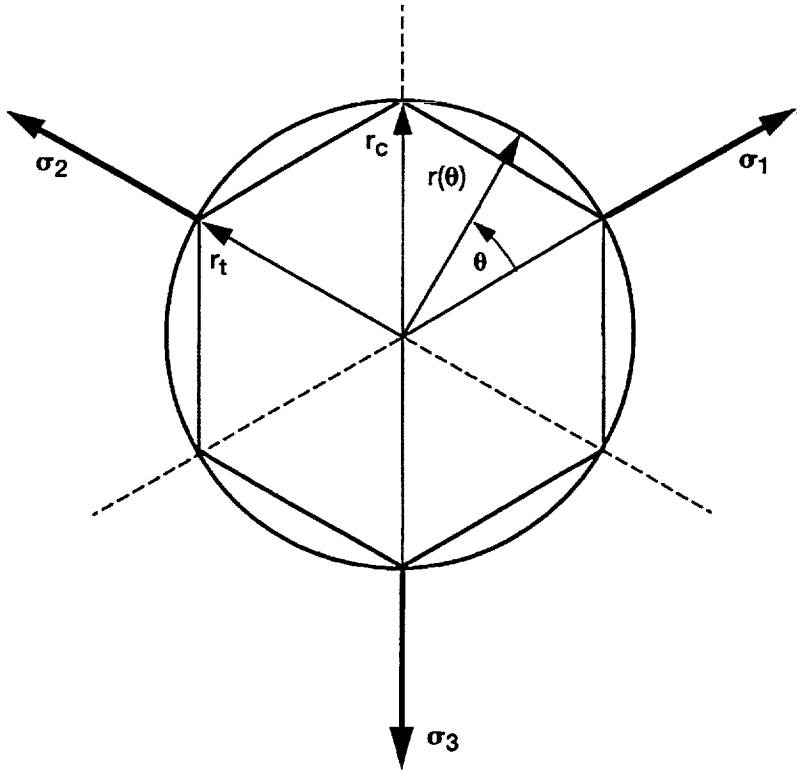

Figure 3.2.—Failure surface depleted in π-plane for a material with equal tensile and compressive strengths.

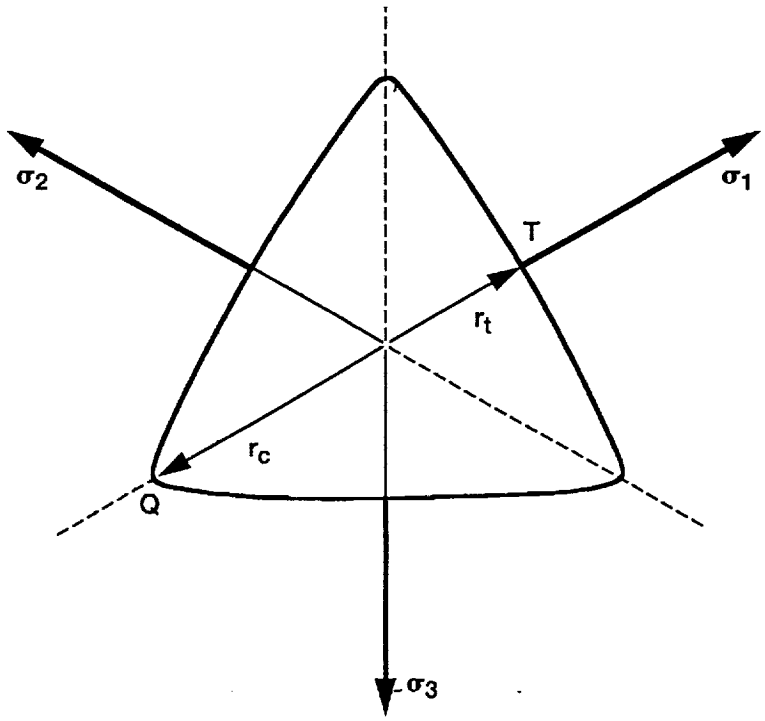

Figure 3.3.—Willam-Warnke failure surface depicted in π-plane.

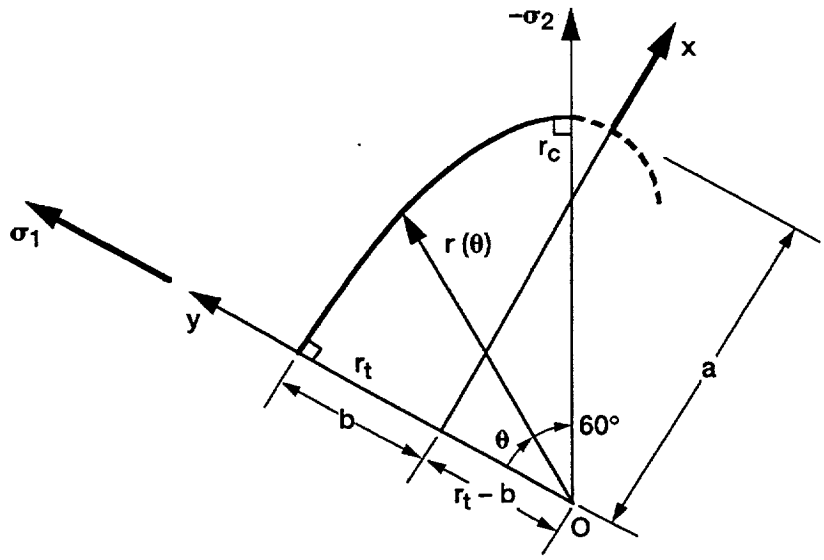

Figure 3.4.—A 60° sector of Willam-Warnke failure surface depicted in π-plane.

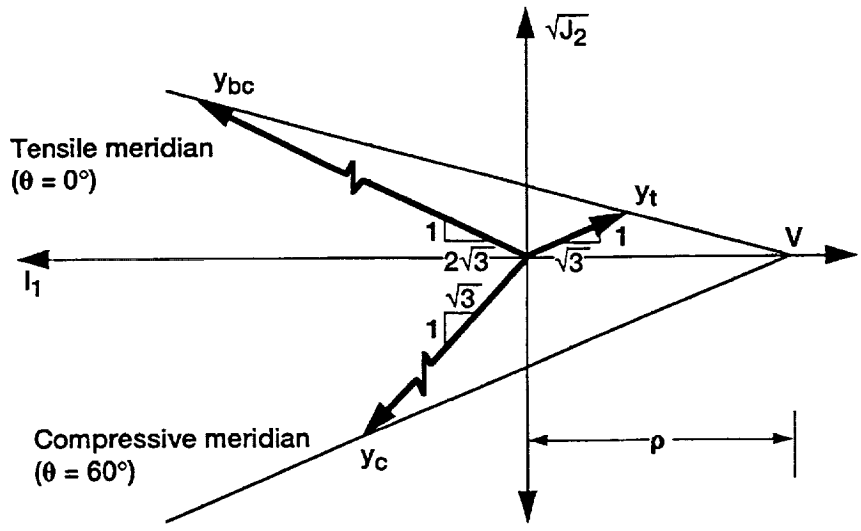

Figure 3.5.—Tensile and compressive meridians viewed in I_1-$\sqrt{J_2}$ stress space.

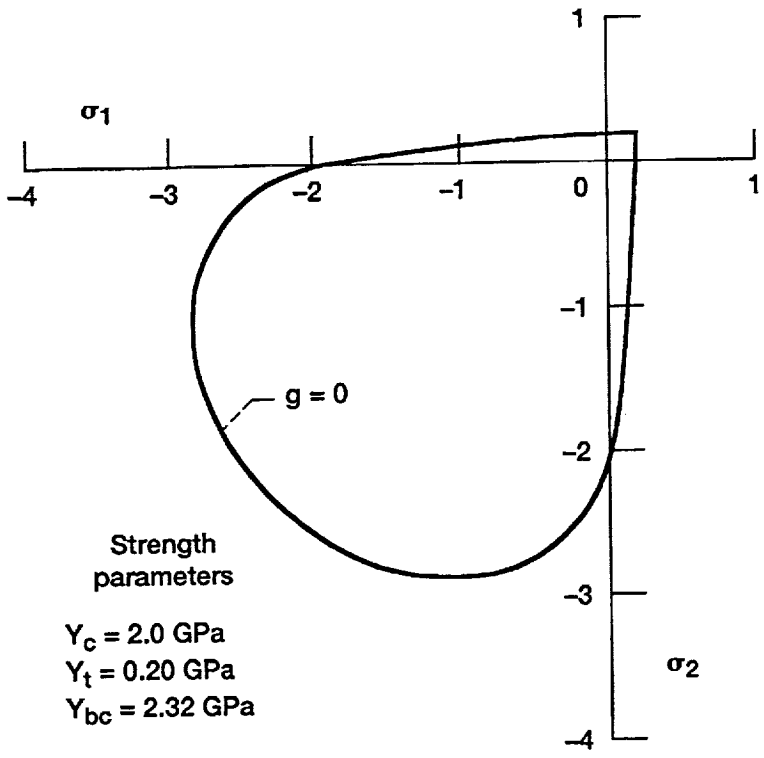

Figure 3.6.—Willam-Warnke failure surface depicted in σ_1–σ_2 stress space.

CHAPTER IV

INTERACTIVE RELIABILITY MODEL

In this chapter the details of transforming the Willam-Warnke failure function into an interactive probabilistic model are presented. Rather than predicting a fail/no fail design condition, this stochastic approach predicts the probability of failure of a component. The design issues discussed here are similar to those outlined in chapter II. The interactive reliability model accounts for a reduction in reliability due to compressive stresses, and also accounts for decreased scatter in failure for compressive stress states in comparison to tensile stress states. Note that the strength parameters used in the Willam-Warnke failure criterion are treated as random variables. Other quantities such as stiffness and loads can be treated in a probabilistic fashion (see Cruse et al., 1988), but since the strength of ceramic-based material systems commonly varies by 100 percent or more, only the strength parameters are treated as random variables.

Reliability is calculated under the assumption that the three strength parameters (Y_c, Y_t, and Y_{bc}) are independent random variables. It is assumed that each parameter is characterized by a two-parameter Weibull distribution (eqs. (2.1) to (2.4)); however, other distributions can be used with this approach. Using separate probability density functions for each random variable is versatile since other statistical distributions such as a three-parameter Weibull distribution or a log-normal distribution can be used to characterize the random variables. The selection of the distribution is always dictated by the failure data. However, for the purpose of simplicity and illustration, only the two-parameter Weibull distribution is considered here. To define the probability density distributions for each strength parameter, a Weibull modulus α and a scale parameter β must be determined experimentally. In general, a significant number of failure tests (a quantity which is dependent on the precision required for the parameter estimates of α and β) are necessary to characterize the probability density function for each random variable. See Pai and Gyekenyesi (1988) for methods of parameter estimation.

Here the functional dependence of the failure function $g(\mathscr{Y}_\alpha, \sigma_{ij})$ is given by equation (3.9). In general the reliability of a unit volume is computed from the expression

$$\mathscr{R} = \text{Probability}\left[g\left(\mathscr{Y}_\alpha, \sigma_{ij}\right) < 0\right] \tag{4.1}$$

where $\mathscr{R}$ represents the reliability. It is assumed that the element is homogeneous in stress; that is, no stress gradients exist throughout the element. Initially, the reliability calculations are based on unit volumes. Later, adjustments that account for arbitrary volumes are introduced. To calculate the reliability for an element of unit volume, the joint density must be integrated over the design space defined by the failure function. This integration takes the form

$$\mathscr{R} = \int_{\partial_s} \int \int \Omega\left(y_c, y_t, y_{bc}\right) dy_c \, dy_t \, dy_{bc} \tag{4.2}$$

where $\Omega\ (y_c, y_t, y_{bc})$ is the joint density function of the random variables that correspond to the material strength parameters, and ∂_s is the design space. By definition, the design space is that portion of the stress space bounded by the failure surface. Under the assumption that the random variables appearing in equation (4.2) are statistically independent, the reliability expression takes the form

$$\mathcal{R} = \int\int_{\partial_s}\int p_1(y_c)p_2(y_t)p_3(y_{bc})dy_c\ dy_t\ dy_{bc} \tag{4.3}$$

where $p_1(y_c)$, $p_2(y_t)$, and $p_3(y_{bc})$ are the marginal probability density functions. These density functions are characterized by the two-parameter Weibull distribution.

The integration defined by equation (4.3) yields the reliability of a unit volume. This type of integration, and the technique for defining the limits of integration were outlined in Sun and Yamada (1978), and Wetherhold (1983). To illustrate the approach, one of the simpler models presented in these references (i.e., the Tsai-Wu criterion) is used as an example since a closed-form solution can be obtained. Application of this type of criterion has been proposed for the analysis of laminate composites, since each ply is analyzed by assuming that the ply is an orthotropic plate subject to plane stress conditions. Here the failure function takes the form

$$\left[\frac{\sigma_1}{Y_1}\right]^2 - \left[\frac{\sigma_1\sigma_2}{Y_1^2}\right] + \left[\frac{\sigma_2}{Y_2}\right]^2 + \left[\frac{\sigma_6}{Y_6}\right]^2 - 1 = 0 \tag{4.4}$$

where σ_1 and σ_2 are in the in-plane normal stresses, and σ_6 is the in-plane shear stress. The strengths Y_1, Y_2, and Y_6 are the random variables associated with the strength in the primary material direction (Y_1), transverse to the primary material direction (Y_2), and an in-plane shear strength (Y_6). The reliability calculation follows the format outlined in equations (4.1) to (4.3), specifically,

$$R = \int_0^w \int_0^{v(Y_6)} \int_0^{u(Y_6,Y_2)} p(y_1)\,p(y_2)\,p(y_6)\,dy_1\,dy_2\,dy_6 \tag{4.5}$$

Here $p(y_1)$, $p(y_2)$, and $p(y_6)$ are the marginal probability density functions for the respective strength variables, and the limits of integration are defined by systematically solving equation (4.4) for each random variable, and then suppressing the random variable. Thus the first limit of integration is defined by the expression

$$u(Y_2, Y_6) = \left[\frac{\sigma_1^2 - \sigma_1\sigma_2}{1^2 - (\sigma_2/Y_2)^2 - (\sigma_6/Y_6)^2}\right]^{1/2} \tag{4.6}$$

Next, terms containing the random variable Y_1 are suppressed in equation (4.4), and the remainder of the equation is solved for Y_2 resulting in

$$v(Y_6) = \left[\frac{\sigma_2^2}{1^2 - (\sigma_6/Y_6)^2}\right]^{1/2} \tag{4.7}$$

To solve for the limits of y_6, terms containing both Y_1 and Y_2 are suppressed in equation (4.4), hence

$$w = \sigma_6 \tag{4.8}$$

Note that each term in this particular failure function (eq. 4.4) contains one strength variable. However, for the Willam-Warnke model each term in the interactive formulation contains all three strength parameters. Deriving the limits would require substitution of equations (3.12), (3.23), (3.24), and (3.25) into equation (3.9), and solving for each of the strength parameters explicitly to obtain expressions similar to equations (4.6) to (4.8). Developing closed-form expressions is intractable because of the definition of $r(\theta)$. For this reason, the triple integral was evaluated using Monte Carlo methods.

The Monte Carlo technique involves generating a uniform random sample of size K for each random variable. A value is selected for each strength parameter via a random number generator. This random number is used with the assumed marginal probability density function (i.e., two-parameter Weibull, three-parameter Weibull, log normal, etc.) to obtain values for the random strength variables. Details of this computational procedure are outlined in Wetherhold (1983). For a given stress state, the failure function is evaluated for each sample of random variables. Initially an element of unit volume subject to a homogeneous stress state is considered. If $g(\mathscr{Y}_\alpha, \sigma_{ij}) < 0$ for a given trial, then that trial is recorded as a success. By repeating this process a suitable number of times for a given state of stress, the reliability (or cumulative distribution) of the element is generated. In essence, the Monte Carlo method provides a means of simulating failure experiments on a computer. This assumes that the marginal probability density functions have been suitably characterized; that is, the values of the α's and the β's are known a priori. For a sufficiently large simulation sample size, reliability is computed by the simple expression

$$\mathscr{R} = \frac{n}{K} \tag{4.9}$$

where n is the number of successful trials (i.e., the number of trials where $g(\mathscr{Y}_\alpha, \sigma_{ij}) < 0$).

Figure 4.1 shows a comparison of the Monte Carlo calculations with the underlying Weibull distribution assumed for the tensile strength random variable. This is a plot of probability of failure versus failure strength. For this case, the reliability of an element of unit volume is given by

$$\mathscr{R} = \exp\left[-\left(\frac{\sigma}{\beta}\right)^\alpha\right] \tag{4.10}$$

where σ is the applied tensile stress. For graphical purposes the natural logarithm of both sides of the expression is taken twice. By introducing a constant C defined as

$$C = \left(\frac{1}{\beta}\right)^\alpha \tag{4.11}$$

then the form of equation (4.10) is

$$\ln\left[\ln\left(\frac{1}{\mathscr{R}}\right)\right] = \ln C + \alpha \ln \sigma \tag{4.12}$$

Here the Weibull shape parameter for tensile strength defines the slope of the line depicted in figure 4.1. For this illustration $\alpha = 5$ and $\beta = 0.2$. The three points represent estimates using the Monte Carlo method for the uniaxial failure strength where the specified reliabilities are 5, 50, and 95 percent. A computer algorithm which

numerically evaluates equation (4.5) using the Monte Carlo technique was used. For this example the desired reliability, the Weibull parameters defining the marginal probability density functions for the strength parameters, and the desired number of Monte Carlo simulations are specified. The simulated tensile load path is described in chapter III. The stress state is increased incrementally along the specified load path until the desired reliability is found to within some predetermined error bound. The data points in figure 4.1 were generated using 100 Monte Carlo trials. As a comparison, figures 4.2 to 4.4 show Monte Carlo estimates for different sample sizes. Figure 4.2 depicts predictions for 500 Monte Carlo trials; figure 4.3, 1000 trials; and figure 4.4, 10 000 trials. Note that as the number of trials increases, the points converge to the line representing the underlying Weibull distribution for the parameter Y_t. This indicates that the numerical approach for evaluating equation (4.5) asymptotically converges to the underlying distribution as the sample size K increases.

To illustrate behavior along other load paths, simulations were conducted for the strength parameters Y_c and Y_{bc}. Figure 4.5 shows the relations for the strength parameter Y_c, and figure 4.6 shows the relations for the parameter Y_{bc}. The Weibull parameters were arbitrarily stipulated. For the uniaxial compressive case, $\alpha = 35$ and $\beta = 2.0$, and for the biaxial compressive case, $\alpha = 35$ and $\beta = 2.32$. Note that the α's were assigned higher values for the compressive strength variables than for the tensile strength variable. Although strength data for isotropic whisker-toughened ceramics are not available, there are sufficient experimental data for monolithic ceramics to indicate that compressive failure modes generally do not exhibit as much scatter as tensile failure modes. It is believed that similar behavior will be exhibited by isotropic whisker-toughened materials. As in the uniaxial tensile case, estimates of reliability for 5, 50, and 95 percent were compared to the linear form of the Weibull equation associated with each load path. Again, all points converged with the line for 10 000 trials.

This technique was also used in calculating the reliability contours shown in figure 4.7. This figure represents the σ_1-σ_2 stress space. The reliability contours represent a homogeneously stressed material element of unit volume. Here the Weibull parameters associated with the tensile strength random variable are arbitrarily chosen to coincide with the example cited in the preceding paragraph, specifically $\alpha_t = 5$ and $\beta_t = 0.2$. Similarly, the Weibull parameters associated with the compressive strength random variable are arbitrarily specified, with $\alpha_c = 35$ and $\beta_c = 2$. Finally the Weibull parameters associated with the equal biaxial compressive strength random variable are $\alpha_{bc} = 35$ and $\beta_{bc} = 2.32$. The three surfaces depicted in figure 4.7 correspond to $\mathcal{R} = 5$, 50, and 95 percent. Note that the reliability contours retain the general behavior of the deterministic failure surface. In general, as the α's increase, the spacing between contours diminishes. Eventually with increasing α the contours would not be distinct and they would effectively map out a deterministic failure surface. An increase in the β's shifts the relative position of the contours in an outward direction indicating an increase in strength. Also note that the α's for the tensile and compressive load paths are different and can be specified independently of each other. This is a distinct advantage relative to the Powers model discussed in chapter II. Since only a tensile Weibull modulus is specified in the Powers model, the same scatter would occur for both tensile and compressive load paths.

The details for computing the reliability of a single element have been presented assuming a homogeneous state of stress and a unit volume. To design a structural component with a varying stress field, the component is discretized and the stress field is characterized using finite element methods. Since component failure may initiate in any of the discrete elements (which typically do not have unit volumes or areas), it is useful to consider a component from a systems viewpoint. A discretized component is a series system if it fails when one of the discrete elements fails. This approach gives rise to weakest-link reliability theories. In a parallel system, failure of a single element does not necessarily cause the component to fail, since the remaining elements may sustain the load through redistribution. Parallel systems lead to what have been referred to in the literature as bundle theories. Since it is assumed that qualitatively the failure behavior of whisker-toughened ceramics mimics monolithic ceramics, a weakest-link reliability theory is adopted for designing structural components.

If the failure of an individual element is considered a statistical event, and these events are assumed to be independent, then the probability of failure of a discretized component is given as

$$P_f = 1 - \prod_{i=1}^{N} R_i \tag{4.13}$$

where N is the number of discrete finite elements for a given component, and R_i is the reliability of the i^{th} discrete element. This reliability is computed in the following manner. Recall that $\mathscr{R}$ (the reliability based on a unit volume) is defined by equations (4.1) to (4.3), but calculated using the Monte Carlo techniques described previously. These same techniques can be used to compute R_i if the Weibull scale parameters are adjusted to reflect the size of the element. In general each scale parameter (β_t, β_c, and β_{bc}) is adjusted by using the following transformation

$$\beta^* = \beta \left[\frac{1}{V_i} \right]^{1/\alpha} \tag{4.14}$$

Here V_i is the volume of the i^{th} element and β^* is the adjusted scale parameter. No adjustment is necessary for the Weibull moduli. The preceding discussion on the reliability model implied that failure of whisker-toughened CMC originates from volume flaws. It is quite possible that component failure is caused by surface and/or volume flaws; that is, competing failure modes may exist. These competing failure modes usually have distinctly different Weibull parameters that characterize the marginal probability density functions. Accordingly, equation (4.14) can be used for surface flaw analyses if V_i is replaced by the area of the i^{th} element, A_i. However, for brevity, only volume flaw analysis is considered here.

This numerical procedure has been incorporated in a public domain test bed computer algorithm given the acronym TCARES (Toughened Ceramics Analysis and Reliability Evaluation of Structures). Currently this algorithm is coupled to the MSC/NASTRAN finite element code. For a complete description of the TCARES algorithm, see Duffy, Manderscheid, and Palko (1989). Before using TCARES, the proposed interactive reliability model that has been implemented into TCARES must be characterized using an extensive data base that includes multiaxial experiments. It is not sufficient to simply characterize the Weibull parameters for each random strength variable. Multiaxial experiments should be conducted to assess the accuracy of the interactive modeling approach. However, once the Weibull parameters have been characterized for each random strength variable, the algorithm allows a design engineer to predict the reliability of a structural component subject to quasi-static multiaxial loads. Isothermal conditions are considered for the application that follows. However, the algorithm is capable of nonisothermal analyses if the Weibull parameters are specified at a sufficient and appropriate number of temperature values. To illustrate certain aspects of the interactive model and the TCARES algorithm, a reliability analysis is performed on a test specimen which is known as the Brazilian disk.

The Brazilian disk is used to circumvent the alignment difficulties encountered in tensile testing brittle materials. In addition the Brazilian disk has been used to determine tensile strengths of brittle materials that exhibit reduced tensile strengths relative to the compressive strength (e.g., concrete and rock). The analytical details concerning the stress field of the Brazilian disk have been discussed by a number of authors including Hondros (1959), Vardar and Finnie (1975), Chong, Smith, and Borgman (1982), and Fessler and Fricker (1984). Most researchers assume that tensile failure usually occurs along the diameter directly beneath the applied load (see fig. 4.8), splitting the disk. However, the region of the disk directly beneath the load experiences very large compressive stress states that dissipate slowly. The interactive model presented here allows for a reduction in reliability when compressive stress states are present. Thus the Brazilian disk can be used to compare the

interactive model with other widely used reliability models that do not account for compressive stress states. For simplicity, the interactive model is compared with the Principle of Independent Action (PIA) reliability model.

It is assumed that the disk is fabricated from an isotropic whisker-toughened CMC material with a Young's modulus of 300 GPa and a Poisson ratio of 0.2. A compressive pressure load of 1000 MPa was applied to the disk, and the subtended angle η for this example is 0.039 rad. The Weibull parameters associated with each random strength variable were arbitrarily chosen. Specifically the Weibull parameters associated with the tensile strength random variable are $\alpha_t = 15$ and $\beta_t = 250$. The Weibull parameters associated with the compressive strength random variable are $\alpha_c = 35$ and $\beta_c = 2500$. Similarly the Weibull parameters associated with the equal biaxial strength random variable are $\alpha_{bc} = 35$ and $\beta_{bc} = 2900$. Note that the β parameters have units of MPa$\cdot$(mm)$^{3/\alpha}$. The disk has a radius of 50 cm and a thickness of 5.0 cm, and was modeled using 1/8 symmetry with 1044 finite elements (see fig. 4.9). The elements used in the structural analysis were 8-node brick elements (MSC/NASTRAN HEX/8). The tensile stress in the x-direction near the center of the disk was 24.8 MPa. This stress remains fairly constant along the vertical diameter, except in the near vicinity of the load, where this stress component changes sign and becomes compressive (see fig. 4.10). The elements near the loads experience large compressive stresses (~997 MPa) in the y-direction that dissipate slowly down the diameter (see fig. 4.11). The stresses in this direction are compressive throughout the disk.

When this particular discretized component was analyzed using the PIA model (with $\alpha = 15$ and $\beta = 250$) the component reliability was 99.9 percent. Note that compressive stress states (specifically compressive principal stresses) do not affect component reliability when using the PIA model. This assumption is similarly adopted for other reliability theories such as Batdorf's reliability model. This lack of accounting for compressive stress states may be a nonconservative assumption depending on the values of the Weibull parameter that characterize the compressive strength random variables. Analyzing the disk using the interactive reliability model presented here resulted in a component reliability of 77.7 percent. Again the Weibull parameters for the compressive strength random variables were arbitrarily specified. However, α values of 35 begin to approach values for metals which have deterministic strength parameters, and an increase in the β values of over an order of magnitude relative to β_t represent conservative estimates of these Weibull parameters. Thus in comparing the component reliability from the PIA model and the interactive reliability model, it is evident that accounting for compressive stress states may play an important role in the analysis of structural components.

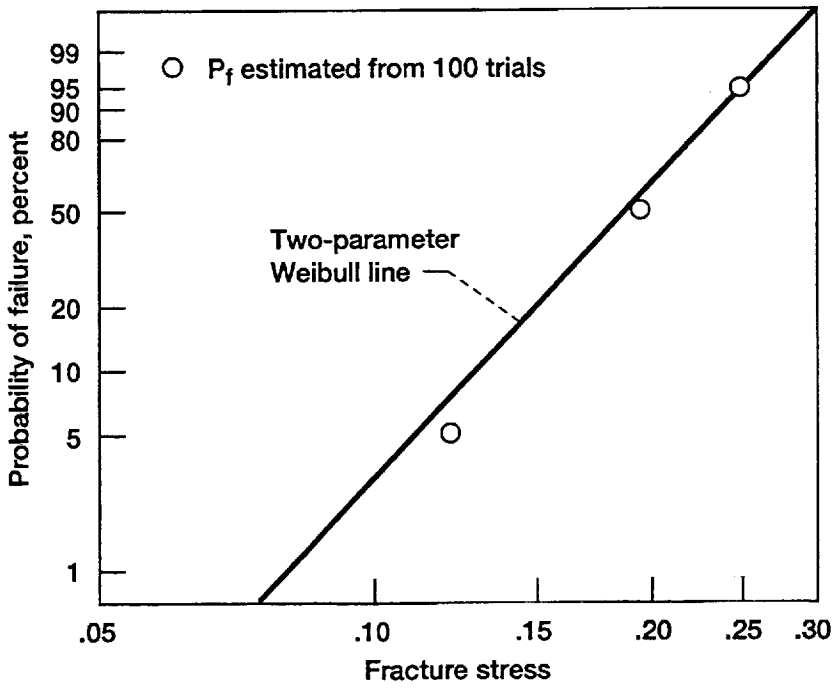

Figure 4.1.—Reliability estimates of uniaxial tensile strengths using 100 Monte Carlo simulations.

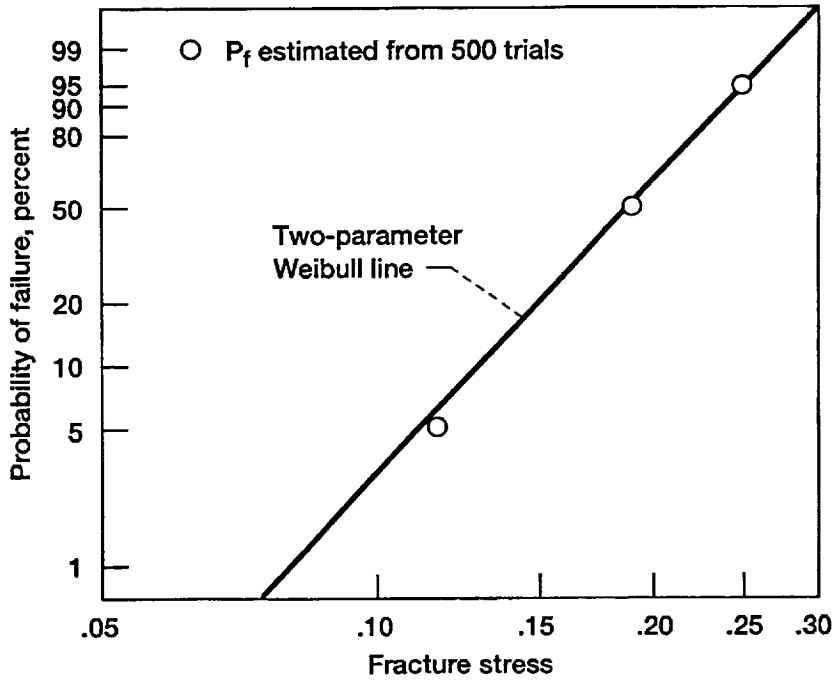

Figure 4.2.—Reliability estimates of uniaxial tensile strengths using 500 Monte Carlo simulations.

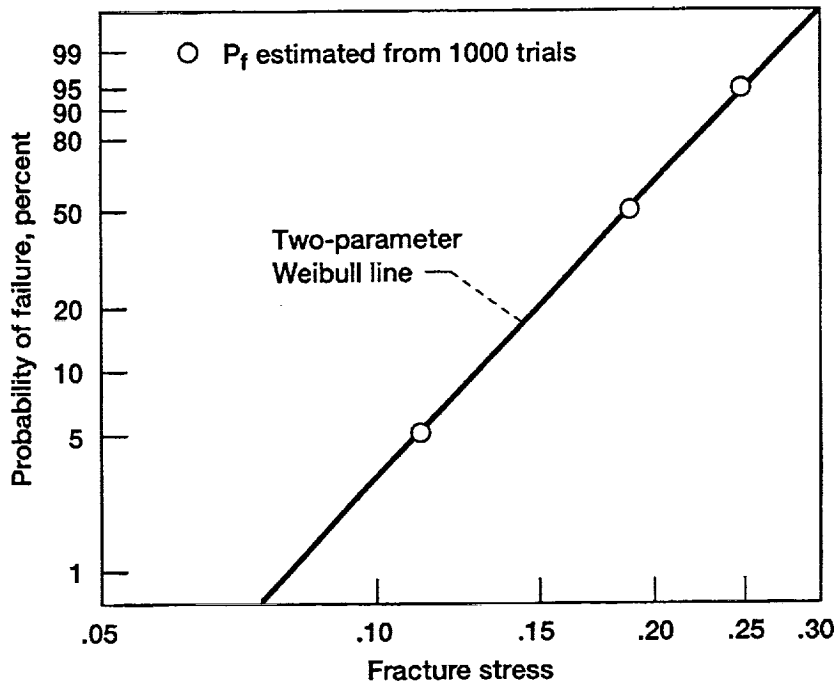

Figure 4.3.—Reliability estimates of uniaxial tensile strengths using 1000 Monte Carlo simulations.

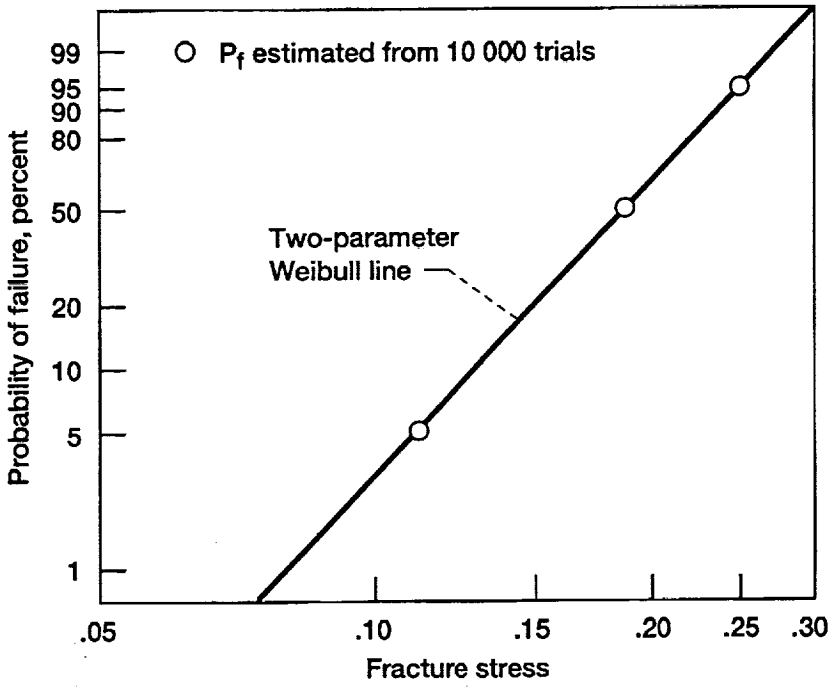

Figure 4.4.—Reliability estimates of uniaxial tensile strengths using 10 000 Monte Carlo simulations.

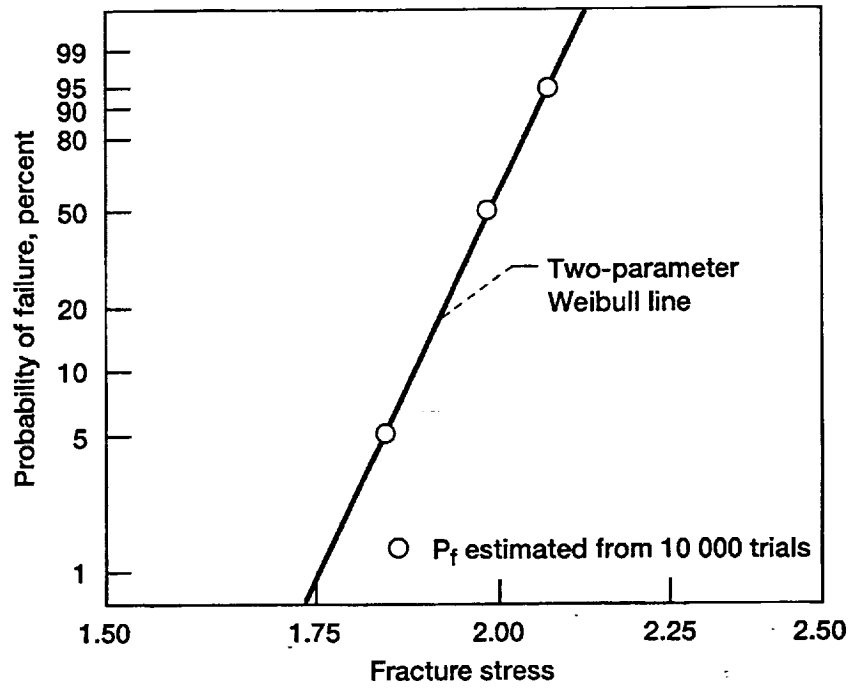

Figure 4.5.—Reliability estimates of uniaxial compressive strengths using 10 000 Monte Carlo simulations.

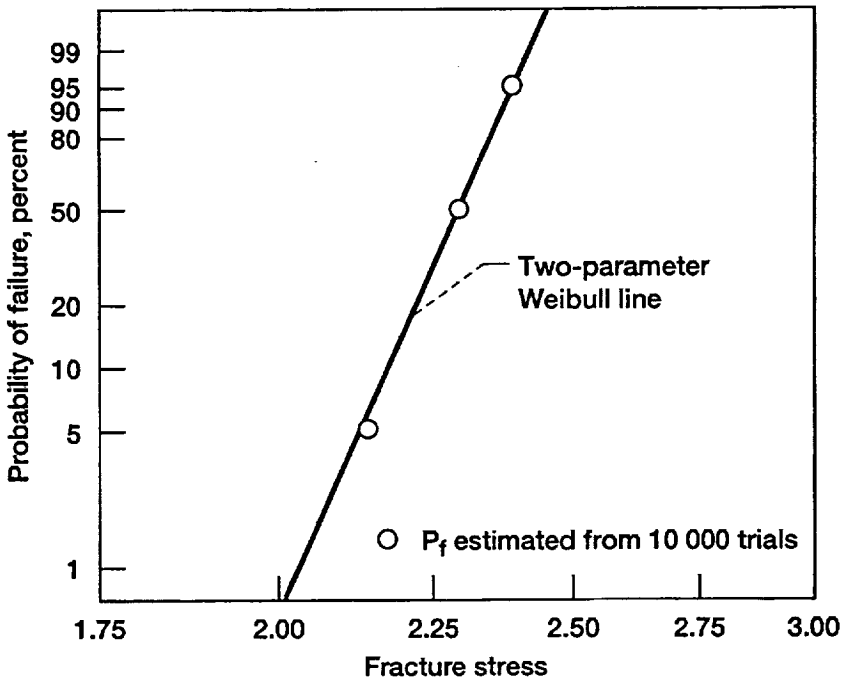

Figure 4.6.—Reliability estimates of biaxial compressive strengths using 10 000 Monte Carlo simulations.

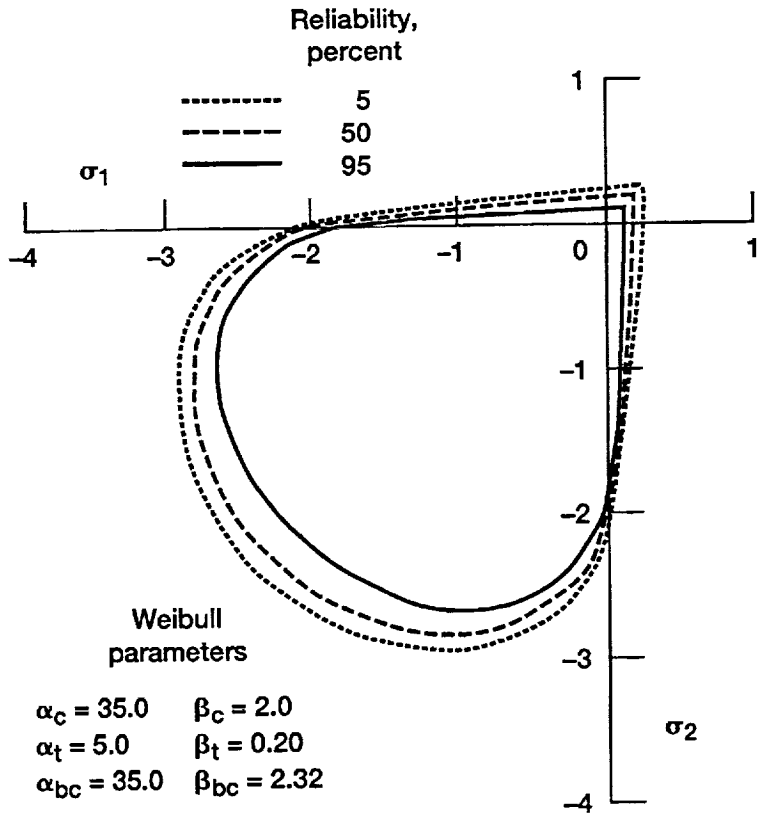

Figure 4.7.—Reliability contours using the reliability model projected onto σ_1–σ_2 stress space.

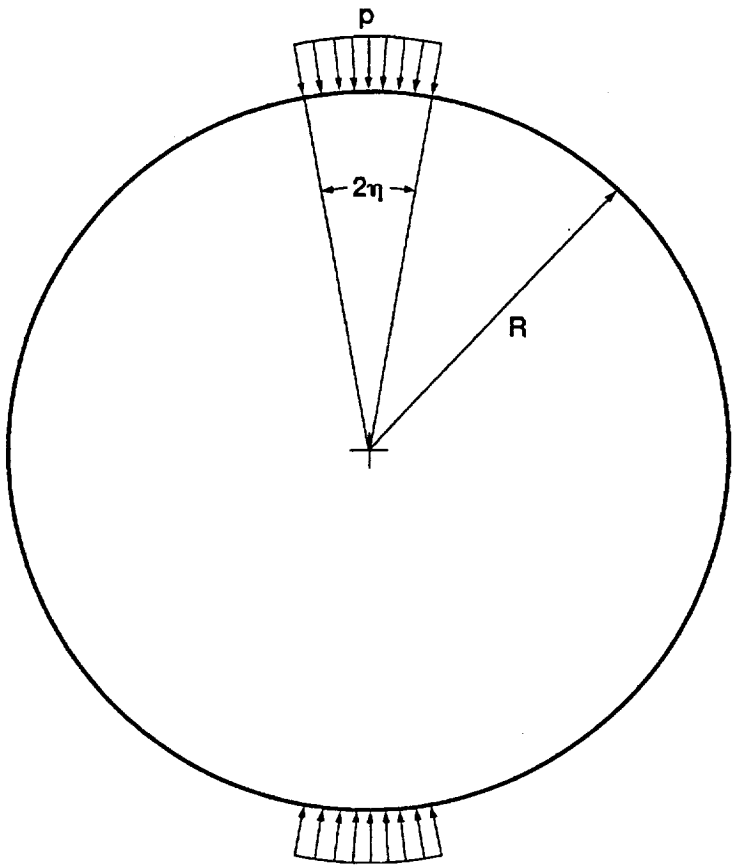

Figure 4.8.—Geometry and pressure load for Brazilian disk test specimen.

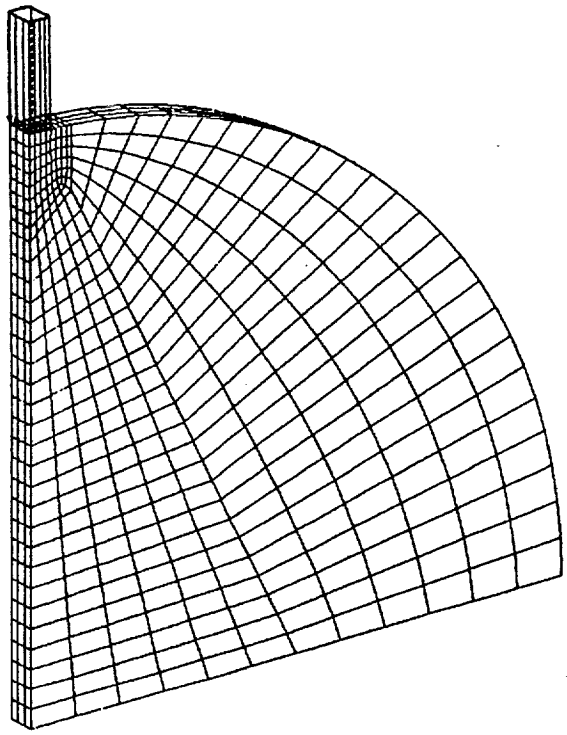

Figure 4.9.—Finite element model for Brazilian disk test specimen.

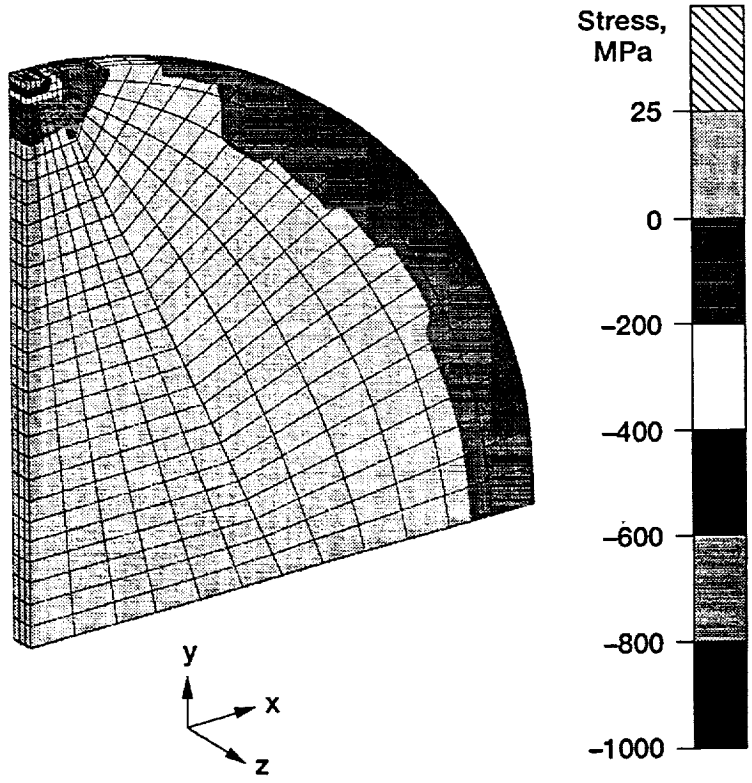

Figure 4.10.—Stresses acting on disk in normal x-direction.

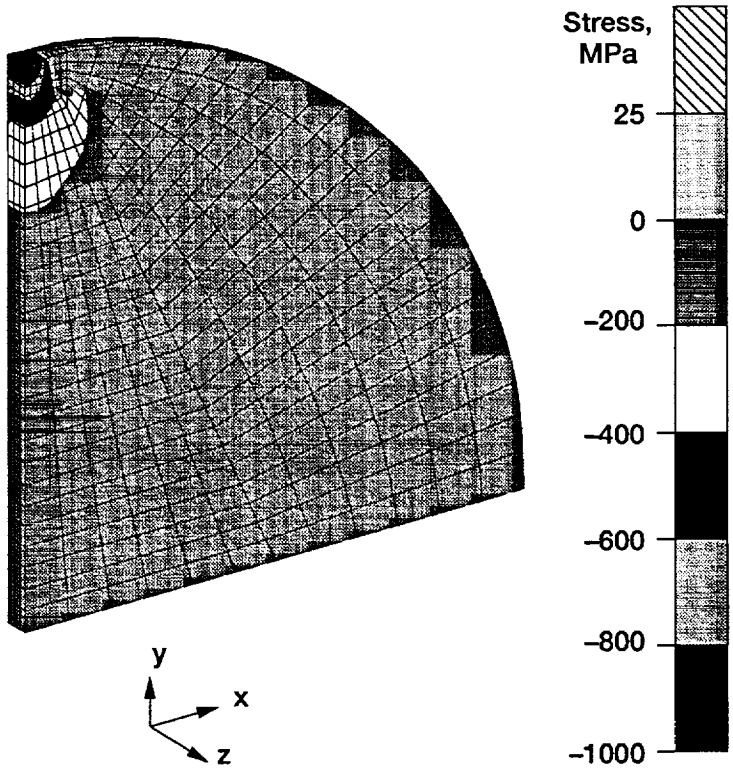

Figure 4.11.—Stresses acting on disk in normal y-direction.

CHAPTER V

CONCLUDING REMARKS AND FUTURE DIRECTION

The basic features of conducting a reliability analysis by deriving an interactive reliability model have been illustrated. The deterministic Willam-Warnke failure criterion serves as the theoretical foundation on which the reliability model was constructed. Fundamental to the work presented here is the assumption that the strength parameters associated with a deterministic failure criterion can be treated as random variables. As a result, the proposed reliability model retains the phenomenological behavior that was present in the deterministic failure criterion, such as sensitivity to hydrostatic stress and reduced tensile strength. The predictive capabilities of the interactive model were examined assuming that the two-parameter Weibull distributions characterized the marginal probability density functions for each random strength variable. This included both uniaxial and multi-axial load paths. The interactive reliability model was implemented into TCARES, a test-bed software program. Since this algorithm has been coupled with a general-purpose finite element program, design engineers are now able to use the code as a postprocessor in order to predict the reliability of a structural component subject to quasi-static multiaxial load conditions. A simple structural problem was presented to illustrate the reliability model and the computer algorithm.

In addition, this type of reliability model can be extended to account for material anisotropy. Using orthotropic materials as an example, the parent deterministic failure function must reflect the stress state (as was done in this report) and the appropriate material symmetry. For orthotropy this requires that

$$g = g\left(\tilde{Y},\ \sigma_{ij},\ a_i,\ b_i\right) \tag{5.1}$$

where a_i and b_i are orthogonal unit vectors that represent the local orthotropic material directions. Because g is a scalar function, it must remain form invariant under arbitrary proper orthogonal transformations. Work by Reiner (1945), Rivlin and Smith (1969), Spencer (1971) and others demonstrated that by applying the Cayley-Hamilton theorem and the elementary properties of tensors, a finite set of invariants (known as an integrity basis) can be derived for scalar functions that are dependent on first- and second-order tensor quantities. See Duffy (1987) for the details regarding the application of the Cayley-Hamilton theorem for this purpose. Form invariance of the scalar functions is ensured if the functions depend on invariants that constitute either the integrity basis, or any subset thereof. A number of authors (Lance and Robinson (1971), Boehler and Sawczuk (1977), Arnold (1989), and Robinson and Duffy (1990)) have used this methodology to develop scalar valued functions that are dependent on stress (a second-order tensor) and material directions (usually characterized by first-order tensors as in eq. (5.1)). Clearly, the future direction alluded to here (i.e., incorporating material symmetry using direction tensors) is not without precedent. However, for anisotropic whisker-toughened ceramic composites the failure function must not only reflect the material anisotropy, but also account for reduced tensile strength, and a dependence on the hydrostatic component of stress, if this behavior is exhibited experimentally.

Recall that the proposed model calculates reliability using the Monte Carlo method. For each stress state 10 000 trials are used to compute reliability. Since this approach is used in conjunction with finite element methods, it could easily challenge the computational capacity of even a supercomputer as the number of discrete finite elements increases. In order to optimize computational efficiency, future work will also concentrate on using numerical schemes referred to as Fast Probability Integration (FPI) techniques. Wu (1984) outlined several fast probability integrators, including the methods of Rackwitz and Fiessler (1978) and Chen and Lind (1982). These are first-order methods since it is assumed that the limit state is linear at the design point. Quadratic methods have been proposed, but the added complexity is not justified by dramatic increases in accuracy. In his work, Wu proposed an improvement to the Rackwitz-Fiessler method. This method uses a least squares

technique to fit an approximated cumulative distribution function for each random variable to the true cumulative distribution. This approach increases accuracy with a minimal increase in computational efforts.

REFERENCES

1. Adams, M.A.: The Strength of Brittle Ceramics in Compressive Stress States. Ph.D. Thesis, University of California, Los Angeles, CA, 1975.

2. Adams, M.; and Sines, G.: A Statistical, Micromechanical Theory of the Compressive Strength of Brittle Materials. J. Am. Ceram. Soc., vol. 61, no. 3-4, 1978, pp. 126-131.

3. Alpa, G.: On a Statistical Approach to Brittle Rupture for Multiaxial States of Stress. Eng. Fract. Mech., vol. 19, no. 5, 1984, pp. 881-901.

4. Arnold, S.M.: A Transversely Isotropic Thermoelastic Theory. NASA TM-101302, 1988.

5. Barnett, R.L., et al.: Fracture of Brittle Materials Under Transient Mechanical and Thermal Loading. Report AFFDL-TR-66-220. IIT Research Institute, Chicago, IL, 1967.

6. Batdorf, S.B.; and Crose, J.G.: A Statistical Theory for the Fracture of Brittle Structures Subjected to Nonuniform States of Stress. J. Appl. Mech., vol. 41, no. 2, 1974, pp. 459-464.

7. Batdorf, S.B.; and Heinisch, H.L., Jr.: Fracture Statistics of Brittle Materials with Surface Cracks. Eng. Fract. Mech., vol. 10, no. 4, 1978, pp. 831-841.

8. Boehler, J.P.; and Sawczuk, A.: On Yielding of Oriented Solids. Acta Mech., vol. 27, no. 1-4, 1977, pp. 185-204.

9. Buljan, S.; Pasto, A.E.; and Kim, H.J.: Ceramic Whisker- and Particulate-Composites: Properties, Reliability, and Applications. Am. Ceram. Bull. vol. 68, no. 2, 1989, pp. 387-394.

10. Chen, W.F.: Plasticity in Reinforced Concrete. McGraw-Hill, New York, 1982.

11. Chen, X.; and Lind, N.C.: A New Method of Fast Probability Integration. Solid Mechanics Division, University of Waterloo, Canada, June 1982.

12. Chong, K.P.; Smith, J.W.; and Borgman, E.S.: Tensile Strengths of Colorado and Utah Oil Shales. J. Energy, vol. 6, no. 2, Mar.-Apr. 1982, pp. 81-85.

13. Clarke, D.: Industrial Applications and Markets for Ceramic Matrix Composites. Rolls-Royce Report No. PNR90753, 1990.

14. Coleman, B.D.: On the Strength of Classical Fibers and Fiber Bundles. J. Mech. Phy. Solids, vol. 7, no. 1, 1958, pp. 60-70.

15. Cooper, N.R.; Margetson, J.; and Humble, S.: Probability of Failure Calculations and Confidence Band Estimates for an Annular Brittle Disc Fractured Under Centrifugal Loading. J. Strain Anal., vol. 21, no. 3, 1986, pp. 121-126.

16. Cruse, T.A., et al.: Probabilistic Structural Analysis Methods For Select Space Propulsion System Structural Components (PSAM). Comput. Struct., vol. 29, no. 5, 1988, pp. 891-901.

17. Daniels, H.E.: The Statistical Theory of the Strength of Bundles of Threads. I. Proc. R. Soc. London A, vol. 183, 1945, pp. 405-435.

18. Duffy, S.F.: A Viscoplastic Constitutive Theory for Transversely Isotropic Metal Alloys. Ph.D. Thesis, University of Akron, Akron, OH, 1987.

19. Duffy, S.F.; and Arnold, S.M.: Noninteractive Macroscopic Reliability Model for Whisker-Reinforced Ceramic Composites. J. Compos. Mater., vol. 24, Mar., 1990, pp. 293-308.

20. Duffy, S.F.; and Manderscheid, J.M.: Noninteractive Macroscopic Reliability Model for Ceramic Matrix Composites with Orthotropic Material Symmetry. J. Eng. Gas Turbines Power, vol. 112, Oct. 1990, pp. 507-511.

21. Duffy, S.F.; Manderscheid, J.M.; and Palko, J.L.: Analysis of Whisker-Toughened Ceramic Components - A design Engineer's Viewpoint. Am. Ceram. Bull., vol. 68, no. 12, 1989, pp. 2078-2083.

22. Fessler, H.; and Fricker, D.C.: Multiaxial Strength Tests for Brittle Materials. J. Strain Anal. Eng. Des., vol. 19, no. 3, 1984, pp. 197-208.

23. Freudenthal, A.M.: Statistical Approach to Brittle Fracture. Fracture, An Advanced Treatise, Vol. 2: Mathematical Fundamentals, H. Liebowitz, ed., Academic Press, New York, 1968, pp. 591-619.

24. Gyekenyesi, J.P.: SCARE - A Post-Processor Program to MSC/NASTRAN for the Reliability Analysis of Ceramic Components. J. Eng. Gas Turbines Power, vol. 108, no. 3, July 1986, pp. 540-546.

25. Harlow, D.G.; and Phoenix, S.L.: Probability Distributions for the Strength of Composite Materials I : Two-Level Bounds. Int. J. Fract., vol. 17, no. 4, 1981, pp. 347-372.

26. Hondros, G.: The Evaluation of Poisson's Ratio and the Modulus of Materials of a Low Tensile Resistance by the Brazilian Test. Aust. J. App. Sci., vol. 10, no. 3, 1959, pp. 243-268.

27. Ikeda, K.; and Igaki, H.: Fracture Criterion for Alumina Ceramics Subjected to Triaxial Stresses. J. Amer. Ceram. Soc., vol. 67, no. 8., 1984, pp. 538-544.

28. Ikeda, K.; Igaki, H.; and Kuroda, T.: Fracture Strength of Alumina Ceramics Under Uniaxial and Triaxial Stress States. Am. Ceram. Bull. vol. 65, no. 4, 1986, pp. 683-688.

29. Lamon, J.: Reliability Analysis of Ceramics Using the CERAM Computer Program. ASME Paper No. 90-GT-98, 1990.

30. Lance, R.H.; and Robinson, D.N.: A Maximum Shear Stress Theory of Plastic Failure of Fiber-Reinforced Materials. J. Mech. Phys. Solids, vol. 19, no. 2, 1971, pp. 49-60.

31. Larsen, R.P.; and Vyas, A.D.: The Outlook for Ceramics in Heat Engines, 1990-2010: Results of a Worldwide Delphi Survey. Report CONF-88-0279-1, Angonne National Lab., II, 1988.

32. Lode, W.: Versuche ueber den Einfuss der mitt leren Hauptspannung auf das Fliessen der Metalle Eisen Kupfer und Nickel. Z. Phys., vol. 36, 1926, pp. 913-939.

33. Midgley, E.; and Pierce, F.T.: Tensile Tests for Cotton Yarns, V. The "Weakest Link" Theorems on the Strength of Long and of Composite Specimens. J. Text. Inst., vol. 17, no. 7, 1926, pp. T335 - T368.

34. Nayak, G.C.; and Zienkiewicz, F.: Convenient Forms of Stress Invariants for Plasticity. J. Struct. Div., vol. 98, no. ST4, Apr. 1972, pp. 949-954.

35. Pai, S.; and Gyekenyesi, J.P.: Calculation of Weibull Strength Parameters and Batdorf Flaw Density Constants for Volume- and Surface-Flaw-Induced Fracture in Ceramics. NASA TM-100890, 1988.

36. Phoenix, S.L.: Probabilistic Concepts in Modeling the Tensile Strength Behavior of Fiber Bundles and Unidirectional Fiber/Matrix Composites. Composite Materials: Testing and Design, Proceedings of the Third Conference, ASTM STP-546, American Society for Testing Materials, Philadelphia, PA, 1974, pp. 130-151.

37. Phoenix, S.L.: Statistical Aspects of Failure of Fibrous Materials. Composite Materials: Testing and *Design*, Proceedings of the Fifth Conference, ASTM STP-674, S.W. Tsai, ed., American Society for Testing Materials, Philadelphia, PA, 1979, pp. 455-483.

38. Powers, L.M.: Reliability-Based Failure Analysis of Brittle Materials. Master's Thesis, Cleveland State University, Cleveland, OH, 1989.

39. Rackwitz, R.; and Fiessler, B.: Structural Reliability Under Combined Random Load Sequences. J. Compos. Struct., vol. 9, 1978, pp. 489-494.

40. Reiner, M.: A Mathematical Theory of Dilatancy. Am. J. Math., vol. 67, 1945, pp. 350-362.

41. Rivlin, R.S.; and Smith, G.F.: Orthogonal Integrity Basis for N Symmetric Matrices. Contributions to Mechanics, D. Abir, ed., Pergamon Press, Oxford, NY, 1969, pp. 121-141.

42. Robinson, D.N.; and Duffy, S.D.: Continuum Deformation Theory for High-Temperature Metallic Composites. J. Eng. Mech., vol. 116, no. 4, 1990, pp. 832-844.

43. Spencer, A.J.M.: Theory of Invariants. Continuum Physics, Vol. I: Mathematics, A. C. Eringen, ed., Academic Press, New York, 1971, pp. 239-255.

44. Sun, C.T.; and Yamada, S.E.: Strength Distribution of a Unidirectional Fiber Composite. J. Compos. Mater., vol. 12, Apr., 1978, pp. 169-176.

45. Vardar, O.; and Finnie, I.: An Analysis of the Brazilian Disk Fracture Test Using the Weibull Probabilistic Treatment of Brittle Strength. Int. J. Fract., vol. 11, no. 3, 1975, pp. 495-508.

46. Weibull, W.: A Statistical Theory of the Strength of Materials. Ing. Vetensk. Akad. Handl., vol. 151, 1939, pp. 5-45.

47. Weibull, W.: A Statistical Distribution Function of Wide Applicability. J. Appl. Mech., vol. 73, no. 3, 1951, pp. 293-297.

48. Wetherhold, R.C.: Statistics of Fracture of Composite Materials Under Multiaxial Loading. Ph.D. Thesis, University of Delaware, Newark, DE, 1983.

49. Willam, K.J.; and Warnke, E.P.: Constitutive Models for the Triaxial Behavior of Concrete. Int. Assoc. Bridge Struct. Eng. Proc., vol. 19, 1975, pp. 1-30.

50. Wu, Y.T.: Efficient Methods for Mechanical and Structural Reliability Analysis and Design. Ph.D. Thesis, The University of Arizona, Tuson, AZ, 1984.

REPORT DOCUMENTATION PAGE

Form Approved
OMB No. 0704-0188

1. AGENCY USE ONLY (Leave blank)	2. REPORT DATE	3. REPORT TYPE AND DATES COVERED
	April 1993	Final Contractor Report

4. TITLE AND SUBTITLE
Interactive Reliability Model for Whisker-Toughened Ceramics

5. FUNDING NUMBERS
WU–778–32–11
NCC3–81

6. AUTHOR(S)
Joseph L. Palko

7. PERFORMING ORGANIZATION NAME(S) AND ADDRESS(ES)

8. PERFORMING ORGANIZATION REPORT NUMBER
E–7513

9. SPONSORING/MONITORING AGENCY NAMES(S) AND ADDRESS(ES)
National Aeronautics and Space Administration
Lewis Research Center
Cleveland, Ohio 44135–3191

10. SPONSORING/MONITORING AGENCY REPORT NUMBER
NASA CR–191048

11. SUPPLEMENTARY NOTES
Project Manager, John P. Gyekenyesi, Structures Division, NASA Lewis Research Center, (216) 433–5587. A similar version of this report was submitted by Joseph L. Palko as a thesis in partial fulfillment of the requirements for the degree Master's of Science in Engineering Mechanics to Cleveland State University, Cleveland, Ohio.

12a. DISTRIBUTION/AVAILABILITY STATEMENT
Unclassified - Unlimited
Subject Category 27

12b. DISTRIBUTION CODE

13. ABSTRACT *(Maximum 200 words)*

Wider use of ceramic matrix composites (CMC) will require the development of advanced structural analysis technologies. This report focuses on the use of an interactive model to predict the time-independent reliability of a component subjected to multiaxial loads. The deterministic, three-parameter Willam-Warnke failure criterion serves as the theoretical basis for the reliability model. The strength parameters defining the model are assumed to be random variables, thereby transforming the deterministic failure criterion into a probabilistic criterion. The ability of the model to account for multiaxial stress states with the same unified theory is an improvement over existing models. The new model has been coupled with a public-domain finite element program through an integrated design program. This allows a design engineer to predict the probability of failure of a component. A simple structural problem is analyzed using the new model, and the results are compared to existing models.

14. SUBJECT TERMS
Whiskers; Ceramics; Composites; Weibull distribution; Interactive; Reliability; Brazilian disk; Finite element analysis

15. NUMBER OF PAGES
48

16. PRICE CODE
A03

17. SECURITY CLASSIFICATION OF REPORT	18. SECURITY CLASSIFICATION OF THIS PAGE	19. SECURITY CLASSIFICATION OF ABSTRACT	20. LIMITATION OF ABSTRACT
Unclassified	Unclassified	Unclassified	